

# Relativistic aspects of orbital and magnetic anisotropies in the chemical bonding and structure of lanthanide molecules

Eite Tiesinga,<sup>1</sup> Jacek Kłos,<sup>2,3</sup> Ming Li,<sup>2</sup> Alexander Petrov,<sup>2,4</sup> and Svetlana Kotochigova<sup>2</sup>

<sup>1</sup>*Joint Quantum Institute, National Institute of Standards and Technology and the University of Maryland, MD 20899, USA*

<sup>2</sup>*Physics Department, Temple University, Philadelphia, PA 19122, USA*

<sup>3</sup>*Joint Quantum Institute, Department of Physics,*

*University of Maryland, College Park MD 20742, USA*

<sup>4</sup>*Saint Petersburg NRC, Kurchatov Institute PNPI, Gatchina, 188300,*

*Russia and Division of Quantum Mechanics, Saint Petersburg University, 199034, Russia*

The electronic structure of magnetic lanthanide atoms is fascinating from a fundamental perspective. They have electrons in a submerged open 4f shell lying beneath a filled 6s shell with strong relativistic correlations leading to a large magnetic moment and large electronic orbital angular momentum. This large angular momentum leads to strong anisotropies, *i. e.* orientation dependencies, in their mutual interactions. The long-ranged molecular anisotropies are crucial for proposals to use ultracold lanthanide atoms in spin-based quantum computers, the realization of exotic states in correlated matter, and the simulation of orbitronics found in magnetic technologies. Short-ranged interactions and bond formation among these atomic species have thus far not been well characterized. Efficient relativistic computations are required. Here, for the first time we theoretically determine the electronic and ro-vibrational states of heavy homonuclear lanthanide Er<sub>2</sub> and Tm<sub>2</sub> molecules by applying state-of-the-art relativistic methods. In spite of the complexity of their internal structure, we were able to obtain reliable spin-orbit and correlation-induced splittings between the 91 Er<sub>2</sub> and 36 Tm<sub>2</sub> electronic potentials dissociating to two ground-state atoms. A tensor analysis allows us to expand the potentials between the atoms in terms of a sum of seven spin-spin tensor operators simplifying future research. The strengths of the tensor operators as functions of atom separation are presented and relationships among the strengths, derived from the dispersive long-range interactions, are explained. Finally, low-lying spectroscopically relevant ro-vibrational energy levels are computed with coupled-channels calculations and analyzed.

## I. INTRODUCTION

A challenging question of molecular chemistry is an accurate description of inter-atomic and inter-molecular bonding at the quantum-mechanical level. This problem has attracted much attention but is not always resolved. Over the last decades, novel perspectives on the problem have relied on ultracold atoms and molecules. For example, quantum degenerate gases of atoms offer a unique platform on which to build and form small molecules in single internal state as they avoid unwanted system complexity. Ultracold gasses of atoms and molecules typically also allow for a high level of control and tunability and are well isolated from their surroundings.

As part of these developments experimental breakthroughs in realizing quantum gases of atoms with large magnetic moments [1–9] have also contributed. These atomic species tend to have a far more complex electronic structure than that of alkali-metal or alkaline-earth species most often studied in the field. The magnetic lanthanides from dysprosium to thulium with their exceptionally large magnetic moments and large orbital momenta are extreme examples of such species. This experimental research relied on controllable and tunable anisotropic dipolar interactions between the atoms. The highly anisotropic short-range interactions between lanthanide atoms, however, remain poorly understood as they require knowledge of their chemical bonds. These systems form an excellent environment for explorations

at the interface between quantum chemistry and atomic and molecular physics.

In previous research, we developed a successful model Hamiltonian to study the anisotropic interactions of bosonic Dy and Er in an external magnetic field [10, 11] and in collaboration with the experimental groups of Drs. Ferlaino and Pfau we found and analyzed hundreds of magnetic Feshbach resonances in their collisions [12–14]. These resonances can be used to convert an atomic gas into a gas of highly-magnetic molecules as well as to study the threshold properties or the ultracold collision-energy dependence of three-body relaxation [15]. These atom-atom interactions have also been studied in thulium (Tm) [16, 17].

In spite of advances in the simulation of ultracold collisional interactions between heavy lanthanide atoms, the fundamental nature of the relativistic bond and short-range electronic states in lanthanide dimers as well as in the even-heavier actinide dimers remains mostly unexplored. Precise knowledge of these interactions is clearly desirable for predicting their quantum vibrations and rotations. There exists an exception though. Substantial progress has been made in understanding interaction in the homonuclear diuranium molecule U<sub>2</sub> [18–21]. The latest studies [20, 21] paid particular attention to the chemical bond of U<sub>2</sub> with its multi-orbital character. Relativistic and correlation effects using the Dirac equation for the electrons were fully incorporated by the authors of Ref. [21] and enabled them to determine the

energies of the lowest electronic states of  $U_2$  in the vicinity of the equilibrium separation. In addition, accurate ground-state potentials for heteronuclear dimer molecules that include one open 4f-shell lanthanide atom and one non-lanthanide atom have become available [22–28].

The bond between two ground-state Er and two ground-state Tm atoms is the focus of this paper. The interactions between the  $j = 6$  Er atoms and between the  $j = 7/2$  Tm atoms are anisotropic and orientation dependent. Here,  $j$  is the total electron angular momentum of an atom. The anisotropy is a consequence of potential energy differences for different relative orientations of the electron angular momenta in the open  $4f^{12}$  and  $4f^{13}$  shells of Er and Tm, respectively. These 4f electrons lie beneath a closed  $6s^2$  shell so that these molecules are chemically similar but have distinct physical properties. Electron motion in lanthanides is strongly correlated and relativistic and spin-orbit coupling is strong.

The ground-state manifold of  $Er_2$  and  $Tm_2$  has a large number of electronic states. They are labeled by projection quantum number  $\Omega$  with values up to  $2j$  of the total dimer electron angular momentum on the symmetry axis of the molecule and well as other selection quantum numbers. Because of this complexity, the intermolecular interactions until now have not been accurately characterized. To fulfill these objectives we have performed, for the first time, relativistic configuration-interaction calculations of all  $\Omega$  states as a function of interatomic separation  $R$  for  $Er_2$  and  $Tm_2$  using the DIRAC code [29]. These configuration-interaction calculations determine the short-range energy splittings among the 91 and 36 distinct adiabatic potentials of the  $Er_2$  and  $Tm_2$  dimers, respectively.

Furthermore, we have setup an analytical spin-coupling or spin-tensor representation of the short-range electronic potential surfaces for their use in determining rotational-vibrational levels in this paper and future improved simulations of the scattering of ultra-cold Er and Tm atoms. This representation has seven spin tensor operators and follows from the analytic form of the long-range anisotropic dispersion or van-der-Waals interaction. We find that the splittings among the  $Er_2$  and  $Tm_2$  potentials are dominated by a single anisotropic dipolar coupling between one of the atomic angular momenta and the mechanical rotation of the atom pair. We have also computed the long-range coupling strengths for the seven tensor operators based on all known atomic transition energies and transition dipole moments of Er and Tm. In fact, we find simple relationships among the seven spin-tensor operators contributing to the long-range interaction Hamiltonian.

Finally, we predict the relativistic Hund’s case (c) structure of the energetically-lowest rotational-vibrational levels of the homonuclear  $Er_2$  and  $Tm_2$  dimers using a discrete-variable representation for the vibrational motion. We hope that our predictions will pave the way to spectroscopic studies of these complex and interesting molecules in the near future.

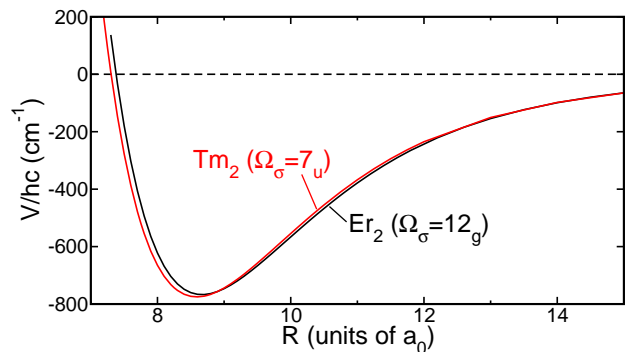


FIG. 1. Potential energies of the energetically-lowest “spin-stretched” states of  $Er_2$  (black curve,  $\Omega_\sigma = 12_g$ ) and  $Tm_2$  (red curve,  $\Omega_\sigma = 7_u$ ) as functions of internuclear separation  $R$ . The calculations are based on non-relativistic configuration-interaction and non-relativistic coupled-cluster theory for  $Er_2$  and  $Tm_2$ , respectively. The zero of energy is at the dissociation limit of two ground-state atoms.

## II. RESULTS AND DISCUSSION

### A. Ground electronic states of $Er_2$ and $Tm_2$ .

In this section we provide the relevant information on molecular electronic properties for two homonuclear lanthanide molecules,  $Er_2$  and  $Tm_2$ , using a two-step approach to determine short-range electronic potential surfaces for all molecular states that dissociate to Er or Tm atoms in the electronic ground states  $[Xe]4f^{12}6s^2(^3H_6)$  and  $[Xe]4f^{13}6s^2(^2F_{7/2})$ , respectively. These electronic configurations contain partially-filled or open submerged 4f and chemically-active 6s atomic orbitals. Computational details and justification of the two step process are presented in Sec. III as well as the Appendices.

In the first step of our study, we focus on the spin-stretched states of  $Er_2$  with  $\Omega_\sigma = 12_g$  and  $Tm_2$  with  $\Omega_\sigma = 7_u$ , where subscripts  $\sigma = g$  and  $u$  for *gerade* or *ungerade* indicate the inversion symmetry of the electron wavefunction with respect to the center of charge. These states have the maximum allowed total electron spin quantum number  $S$  and the maximum projection quantum number  $\Lambda$  of the total electron orbital angular momentum along the internuclear axis, corresponding to the  $S = 2, \Lambda = 10$  and  $S = 1, \Lambda = 6$  states for  $Er_2$  and  $Tm_2$ , respectively. We have used non-relativistic configuration-interaction or coupled-cluster calculations to determine an accurate depth for the potential energy of these spin-stretched states.

Figure 1 shows the spin-stretched potential energy curves for  $Er_2$  and  $Tm_2$  as functions of interatomic separation  $R$ . The relatively shallow potential depths of just under  $hc \times 800 \text{ cm}^{-1}$  reflects the covalent bond of the two closed  $6s^2$  orbitals. The equilibrium separations at the potential minima are  $R_e = 8.7a_0$  and  $8.6a_0$  for  $Er_2$  and  $Tm_2$ , respectively. Here,  $h$  is Planck’s constant,  $c$  is the speed of light in vacuum, and  $a_0 = 0.0529177 \text{ nm}$  is

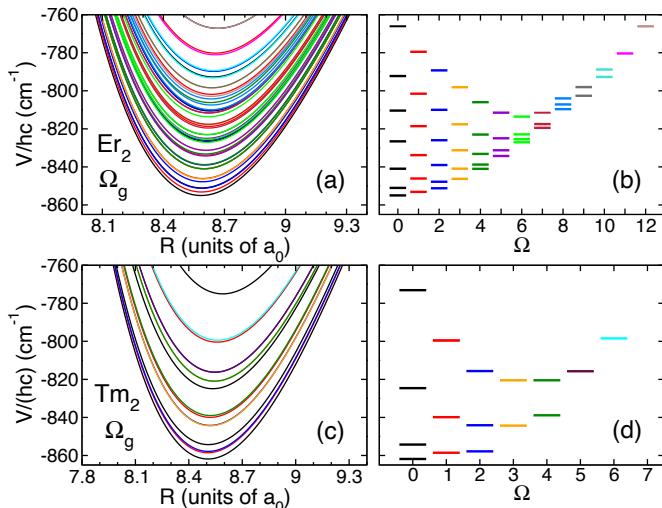


FIG. 2. Relativistic  $\Omega_g^\pm$  potential energy curves with *gerade* symmetry for  $\text{Er}_2$  (panel a) and  $\text{Tm}_2$  (panel c) as functions of internuclear separation  $R$  near the equilibrium separation as obtained from electronic structure calculations. All potentials approach zero energy for  $R \rightarrow \infty$ . Panels (b) and (d) show potential energies from panels (a) and (c) using the same line colors at the equilibrium separation as functions of projection quantum number  $\Omega$  for  $\text{Er}_2$  and  $\text{Tm}_2$ , respectively. *Gerade*  $\Omega = 0$  states are  $0^+$  states. Potentials of states with  $\Omega$  and  $-\Omega$  are degenerate.

the Bohr radius. The depth and shape of these potentials is similar to that of the  $X^1\Sigma_g^+$  state of the non-magnetic  $\text{Yb}_2$  [30].

In a second step, we determine energy splittings among the  $\text{Er}_2$  and  $\text{Tm}_2$  potentials, using fully-relativistic configuration-interaction method implemented into DIRAC 2019 [29] that includes spin-orbit and anisotropic short-range interactions between atoms with two open 4f shells. The states are described by the projection quantum number of the total electronic angular momentum  $\vec{j}_{\text{el}} = \vec{j}_1 + \vec{j}_2$  on the internuclear axis  $\Omega$ , the *gerade* and *ungerade* symmetry, and a parity symmetry for  $\Omega = 0$  states. Here,  $\Omega$  ranges from 0 to 12 for  $\text{Er}_2$  and 0 to 7 for  $\text{Tm}_2$  and labeling  $\Omega^\pm = 0^+$  or  $0^-$  indicates a symmetry with respect to the reflection of the electron wavefunction through a plane containing the internuclear axis.

Figures 2(a) and (c) show the *gerade* relativistic potential energy surfaces (PES) for  $\text{Er}_2$  and  $\text{Tm}_2$  as functions of internuclear separation near their equilibrium separation. There are 49 *gerade* potentials for  $\text{Er}_2$  and 16 for  $\text{Tm}_2$ . For the separations shown in the figure and, in fact, for larger separations the splittings are less than 10% of the depth of the potentials relative to the dissociation energy. The figures for the *ungerade* states is qualitatively similar and reproduced in the Appendices. There are 42 and 20 *ungerade* potentials for  $\text{Er}_2$  and  $\text{Tm}_2$ , respectively.

The splittings among the *gerade* relativistic potentials seem at first glance nontrivial. A pattern, however,

emerges when we plot the potential energies at a single  $R$  near the equilibrium separation as functions of projection quantum number  $\Omega$ , see Figs. 2(b) and (d). For both dimers the energetically lowest potential is a  $0_g^+$  state. We also observe that the splittings among states with the same  $\Omega$  gradually decrease with increasing  $\Omega$ . In fact, the potential energies at the equilibrium separation are arranged in parabolic shapes. Finally, for  $\text{Er}_2$  the  $0_g^+$  state with the smallest well depth is nearly degenerate with the spin stretched  $12_g$  state. A discussion of the origin of this pattern is given in the following subsection. Please note that the  $\Omega = 7$  state for  $\text{Tm}_2$  has *ungerade* symmetry.

## B. Spin tensor decomposition of $\text{Er}_2$ and $\text{Tm}_2$ PESs.

A tensor decomposition of the potential energy surfaces enables us to write PESs as weighted sums of spin-spin coupling terms. It removes the need for a complicated evaluation of non-adiabatic couplings among potentials. We believe that the tensor format is essential for our molecular systems with their tens to hundred adiabatic channel potentials in the ground configuration.

Here, we apply the tensor decomposition technique developed in our previous study of scattering dynamics between ultracold Dy atoms [10] assuming that the molecular electronic wavefunction is well represented by superpositions of (anti)symmetrized, parity-conserving products of atomic electronic ground states  $|j_i m_i\rangle$  or  $|j_i \Omega_i\rangle$  for atom  $i = 1, 2$ . Atomic states are labeled by eigenvalues of the total electronic angular momentum operator  $\vec{j}_i$ , where projection quantum numbers along a space-fixed quantization axis are denoted by  $m_i$  and those along the body-fixed internuclear axis by  $\Omega_i$ . For homonuclear systems  $j_1 = j_2 \equiv j$ . Nevertheless, subscripts 1 and 2 on operators  $\vec{j}_i$  and atomic states are kept to indicate the appropriate atom. (As always we omit the reduced Planck constant  $\hbar$  in describing the eigenvalues of angular momentum operators.)

The atom-atom interactions are then expressed as a sum of isotropic and anisotropic spin-tensor interactions. In principle, an infinite number of such interactions of ever increasing complexity exist. We, however, only include the seven low-rank tensors that describe the van-der-Waals interaction at large interatomic separations [10]. These are

$$V(\vec{\mathbf{R}}) = \sum_{k=0,2,4} \sum_{i=1}^{N_k} V_k^{(i)}(R) \sum_{q=-k}^k (-1)^q T_{kq}^{(i)} C_{k,-q}(\hat{\mathbf{R}}) \quad (1)$$

with rank- $k$  spherical tensor operators  $T_{kq}^{(i)}$  with components  $q$ , spherical harmonic functions  $C_{kq}(\hat{\mathbf{R}})$  with  $C_{kq}(\hat{\mathbf{0}}) = \delta_{q0}$ , and  $\hat{\mathbf{R}}$  is the orientation of the interatomic axis. Here,  $\delta_{ij}$  is the Kronecker delta. The seven  $T_{kq}^{(i)}$

correspond to three isotropic rank-0 tensors

$$\hat{T}_{00}^{(1)} = I, \quad (2)$$

$$\hat{T}_{00}^{(2)} = [j_1 \otimes j_2]_{00} / \hbar^2, \quad (3)$$

$$\hat{T}_{00}^{(3)} = [[j_1 \otimes j_1]_2 \otimes [j_2 \otimes j_2]_2]_{00} / \hbar^4, \quad (4)$$

three anisotropic rank-2 tensors

$$\hat{T}_{2q}^{(1)} = [j_1 \otimes j_1]_{2q} / \hbar^2 + [j_2 \otimes j_2]_{2q} / \hbar^2, \quad (5)$$

$$\hat{T}_{2q}^{(2)} = [j_1 \otimes j_2]_{2q} / \hbar^2, \quad (6)$$

$$\hat{T}_{2q}^{(3)} = [[j_1 \otimes j_1]_2 \otimes [j_2 \otimes j_2]_2]_{2q} / \hbar^4, \quad (7)$$

and a single anisotropic rank-4 tensor

$$\hat{T}_{4q}^{(1)} = [[j_1 \otimes j_1]_2 \otimes [j_2 \otimes j_2]_2]_{4q} / \hbar^4. \quad (8)$$

Thus  $N_0 = 3$ ,  $N_2 = 3$ , and  $N_4 = 1$  in Eq. (1). We have followed the  $\otimes$  notation of Ref. [31] for combining spherical tensor operators, which is equivalent to the notation used in Ref. [32]. Then  $I$  is the identity operator, and  $[j_1 \otimes j_2]_{kq}$  denotes a tensor product of angular momentum operators  $\bar{j}_1$  and  $\bar{j}_2$  coupled to an operator of rank  $k$  and component  $q$ . Finally,  $V_k^{(i)}(R)$  are  $R$ -dependent strengths with units of energy.

The eigenvalues of the interaction operator  $V(\vec{\mathbf{R}})$  as functions of  $R$  correspond to the adiabatic electronic potentials. The corresponding eigenstates are  $R$ -dependent superpositions of  $|j_1 \Omega_1\rangle |j_2 \Omega_2\rangle + \epsilon \sigma |j_2 \Omega_2\rangle |j_1 \Omega_1\rangle$  (excluding normalization) with the constraints that  $\Omega = \Omega_1 + \Omega_2 \geq 0$  and *gerade/ungerade* inversion symmetry are conserved. Here,  $\sigma = +1/-1$  for *gerade/ungerade* states and  $\epsilon = +1/-1$  for Er and Tm, respectively.

We obtain the strengths  $V_k^{(i)}(R)$  by a least-squares procedure minimizing the differences of the splittings with respect to the spin-stretched potential. We only do so for separations  $R \leq 12a_0$  for which DIRAC 2019 converged. All  $V_k^{(i)}(R)$  except  $V_{k=0}^{(1)}(R)$  and  $V_{k=2}^{(1)}(R)$  are consistent with zero. Thus, the dominant spin-tensor operators are either spin independent or a rank-2 tensor operator, corresponding to an  $R$ -dependent effective atomic quadrupole moment coupled to the rotation of the dimer. The spin-independent strength  $V_{k=0}^{(1)}(R)$  closely follows the spin-stretch potential shown in Fig. 1. See the Appendices for our recommended choice to construct the seven  $V_k^{(i)}(R)$ , for uncertainty budgets, and for the procedure to construct strengths for  $R > 12a_0$ .

The fitted  $V_{k=2}^{(1)}(R)$  for Er<sub>2</sub> and Tm<sub>2</sub> are shown in Fig. 3 as functions of  $R$  up to  $12a_0$ . The anisotropic strength is positive, is at most a few times  $\hbar c \times 1 \text{ cm}^{-1}$ , and approaches zero for large  $R$ . Finally, these anisotropic strengths are at least two orders of magnitude smaller than  $V_{k=0}^{(1)}(R)$ . Tables with values for  $V_{k=0}^{(1)}(R)$  and  $V_{k=2}^{(1)}(R)$  can be found in the Appendices.

The dominance of the isotropic spin-independent tensor operator is a consequence of the fact that the spatial extent of the 4f orbital is much smaller than that of the

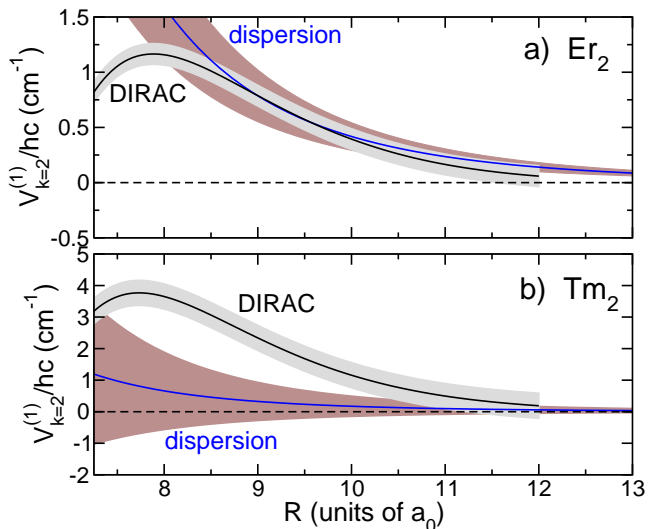


FIG. 3. The fitted anisotropic spin-tensor strength  $V_{k=2}^{(1)}(R)$  for Er<sub>2</sub> (panel a) and Tm<sub>2</sub> (panel b) as a function of  $R$  (black curve labeled DIRAC with gray one-standard-deviation uncertainty band). The strength is compared to the van-der-Waals dispersion potential  $C_{k=2}^{(1)}/R^6$  (blue curve with brown one-standard-deviation uncertainty band).

6s orbital. In fact, the 4f orbital of one atom does not significantly overlap with that of a nearby Er or Tm atom even for  $R$  near the equilibrium separation.

We can now explain the origin of the patterns seen in Fig. 2. Including only the two dominant spin tensor operators in  $V(\vec{\mathbf{R}})$ , eigenstates of  $V(\vec{\mathbf{R}})$  correspond to *single*  $|j_1 \Omega_1\rangle |j_2 \Omega_2\rangle + \epsilon \sigma |j_2 \Omega_2\rangle |j_1 \Omega_1\rangle$  states. They have eigenenergies

$$V(R; \Omega) = V_{k=0}^{(1)}(R) + V_{k=2}^{(1)}(R) \frac{3(\Omega_1^2 + \Omega_2^2) - 2j(j+1)}{\sqrt{6}}. \quad (9)$$

with quadratic or parabolic dependences on  $\Omega_1$  and  $\Omega_2$  (and thus  $\Omega$ ). For Er<sub>2</sub> with positive  $V_{k=2}^{(1)}(R)$  and integer  $j$ , Eq. (9) predicts that the  $\Omega_1 = \Omega_2 = 0$  state and thus an  $\Omega = 0$  state has the lowest potential energy. In fact, for Er<sub>2</sub> this is a  $0_g^+$  state. In addition, Eq. (9) implies that the energetically-highest  $\Omega = 0$  state is degenerate with the sole spin-stretched  $\Omega = 12$  state. In fact, multiple degenerate adiabatic states with the same value for  $\Omega_1$  but opposite-signed values for  $\Omega_2$  exist.

For Tm<sub>2</sub> also with positive  $V_{k=2}^{(1)}(R)$  but now half-integer  $j$ , the model is quite satisfactory as well. Equation (9) predicts that states with  $|\Omega_1| = |\Omega_2| = 1/2$  have the lowest energy. In this case,  $\Omega_\sigma$  is either  $0_g^+$  or  $0_u^-$  (both with  $\Omega_1 = -\Omega_2 = 1/2$ ) or  $1_u$  (with  $\Omega_1 = \Omega_2 = 1/2$ ) and the ground state should be three-fold degenerate. In fact, the energetically-lowest level from the DIRAC calculations is a  $0_g^+$  state. Any removal of degeneracies is due to one or more of the five weaker spin-tensor operators not accounted for in Eq. (9).

Although the five weaker spin-tensor operators could

not be reliably extracted from the least-squares adjustment to *all* splittings among the relativistic potentials of  $\text{Tm}_2$ , additional analyses show that the spin-tensors in Eqs. (3) and (6) are the most important of the five. The first-order correction to the energy due to these two spin-tensor operators is

$$\left(-\frac{1}{\sqrt{3}}V_0^{(2)}(R) + \frac{2}{\sqrt{6}}V_2^{(2)}(R)\right)\Omega_1\Omega_2 \quad (10)$$

with a positive value within the parenthesis. Thus the  $0_g^+$  state has a lower potential energy than the  $1_u$  state.

### C. Spin-tensors for long-range interactions.

The results shown in Figs. 2 and 3 focused on the deepest parts of the potentials. For scattering of ultracold atoms the long-range or large  $R$  part of the potential is equally important. The long-range form involves the van-der-Waals as well as magnetic and quadrupolar interactions.

In our model for  $V(\vec{\mathbf{R}})$  all seven strengths  $V_k^{(i)}(R)$  have a  $C_k^{(i)}/R^6$  contribution for  $R \rightarrow \infty$ . Here,  $C_k^{(i)}$  are van-der-Waals coefficients. The  $k=2, i=2$  strength has a second long-range contribution. That is,  $V_2^{(2)}(R) \rightarrow D_2^{(2)}/R^3 + C_2^{(2)}/R^6$ , where  $D_2^{(2)}/R^3$  describes the magnetic dipole-dipole interaction between the magnetic moments of the lanthanides atoms. Its strength  $D_2^{(2)}$  is  $-\sqrt{6}\alpha^2(g_j/2)^2 E_h a_0^3$ , where  $g_j$  is the electronic  $g$ -factor of the atomic ground state,  $\alpha$  is the fine-structure constant, and  $E_h = 4.35974 \times 10^{-18}$  J is the Hartree energy. The magnetic dipole-dipole interaction is not captured by electronic structure calculations, but is relevant for scattering calculations.

The rank-4 strength  $V_{k=4}^{(1)}(R)$  has a second long-range contribution as well. It approaches  $Q_4^{(1)}/R^5 + C_4^{(1)}/R^6$  for large  $R$  with a  $1/R^5$  quadrupole-quadrupole term with coefficient  $Q_4^{(1)} = 6\sqrt{70}(\mathcal{Q}/ea_0^2)^2/[j_i^2(2j_i-1)^2] \times E_h a_0^5$  for homonuclear dimers that is solely determined by the atomic quadrupole moment  $\mathcal{Q} = \langle j_i j_i | Q_{20} | j_i j_i \rangle$  of the  $m_i = j_i$  spin-stretched state of Er or Tm [33] and  $e$  is the positive elementary charge. The quadrupole moment for erbium was calculated in our previous paper [12] and equals  $0.029ea_0^2$ . For thulium  $\mathcal{Q}$  is not available, but expected to be equally small compared to  $ea_0^2$ . For vibrational simulations with thulium we use  $\mathcal{Q} = 0$ .

We have determined the  $C_k^{(i)}$  coefficients for  $\text{Er}_2$  and  $\text{Tm}_2$  from second-order perturbation theory in the electric dipole-dipole interaction using experimentally-determined atomic transition frequencies and oscillator strengths or Einstein  $A$  coefficients as well as their reported uncertainties. We closely follow the calculations in Refs. [10, 34] for the dysprosium dimer. The evaluation of the seven van-der-Waals coefficients is described in the Appendices. Values are given in Table I, while correlation coefficients are given in the Appendices. The relative

TABLE I. Isotropic and anisotropic van-der-Waals dispersion coefficients  $C_k^{(i)}$  for Er + Er and Tm + Tm sorted by value and then by rank  $k$ . The first three columns label the seven tensor operators. The last two columns give their value and its one-standard-deviation statistical uncertainties. The strength of tensor operator  $[j_1 \otimes j_2]_2$  is  $\sqrt{2}$  times larger than that of  $[j_1 \otimes j_2]_0$ . Similarly, the strengths of the last three tensor operators of each dimer are related by simple algebraic factors discussed in the text. For numerical convenience the strengths are given with additional digits.

Homonuclear Erbium dimer				
$k$	$i$	Operator $T_k^{(i)}$	$C_k^{(i)}$ (units of $E_h a_0^6$ )	$u(C_k^{(i)})$
0	1	$I$	-1723.072 389 927	65.
2	1	$[j_1 \otimes j_1]_2 + [j_2 \otimes j_2]_2$	1.903 660 883	0.57
0	2	$[j_1 \otimes j_2]_0$	0.171 750 953	0.099
2	2	$[j_1 \otimes j_2]_2$	0.242 892 527	0.14
0	3	$[[j_1 \otimes j_1]_2 \otimes [j_2 \otimes j_2]_2]_0$	-0.000 943 784	0.00055
2	3	$[[j_1 \otimes j_1]_2 \otimes [j_2 \otimes j_2]_2]_2$	-0.001 128 037	0.00066
4	1	$[[j_1 \otimes j_1]_2 \otimes [j_2 \otimes j_2]_2]_4$	-0.009 080 527	0.0053

Homonuclear Thulium dimer				
$k$	$i$	Operator $T_k^{(i)}$	$C_k^{(i)}$ (units of $E_h a_0^6$ )	$u(C_k^{(i)})$
0	1	$I$	-1672.115 030 649	54.
2	1	$[j_1 \otimes j_1]_2 + [j_2 \otimes j_2]_2$	0.788 488 761	1.47
0	2	$[j_1 \otimes j_2]_0$	0.001 566 976	0.012
2	2	$[j_1 \otimes j_2]_2$	0.002 216 039	0.017
0	3	$[[j_1 \otimes j_1]_2 \otimes [j_2 \otimes j_2]_2]_0$	-0.000 309 025	0.00060
2	3	$[[j_1 \otimes j_1]_2 \otimes [j_2 \otimes j_2]_2]_2$	-0.000 369 355	0.00072
4	1	$[[j_1 \otimes j_1]_2 \otimes [j_2 \otimes j_2]_2]_4$	-0.002 973 250	0.0058

sizes of the  $C_k^{(i)}$  reinforce the observations regarding the strengths  $V_k^{(i)}(R)$  derived from the electronic structure calculations

For  $\text{Er}_2$  we observe that the absolute value of the magnetic dipole-dipole interaction  $|D_2^{(2)}|/R^3$  equals  $C_2^{(1)}/R^6$  at  $R \approx 35a_0$  and  $C_2^{(2)}/R^6$  at  $R \approx 18a_0$ . Hence, for  $R \gg 35a_0$  the magnetic dipole-dipole interaction is the strongest anisotropic interaction, while for smaller  $R$  the effective quadrupole interaction of Eq. (5) is the strongest anisotropic interaction.

Less obvious from Table I is that we have been able to derive non-trivial algebraic relationships among the  $C_k^{(i)}$  thereby reducing the number of independent dispersion coefficients from 7 to 4. We find that

$$C_2^{(2)} = \sqrt{2}C_0^{(2)} \quad (11)$$

showing that the spin-exchange strength and the effective dipole-dipole strength multiplying Eqs. (3) and (6), respectively, are related. Similarly, we find that

$$C_2^{(3)} = \sqrt{\frac{10}{7}}C_0^{(3)} \quad \text{and} \quad C_4^{(1)} = 6\sqrt{\frac{18}{7}}C_0^{(3)} \quad (12)$$

relating the strengths of the three spin-tensors constructed from the two effective atomic quadrupole op-

erators  $[j_1 \otimes j_1]_2$  and  $[j_2 \otimes j_2]_2$ . The derivation of these relations can be found in the Appendices.

#### D. Ro-vibrational eigenstates.

We finish our analyses of  $\text{Er}_2$  and  $\text{Tm}_2$  by computing their energetically-lowest ro-vibrational eigenstates. That is, we compute eigenstates of  $-\hbar^2\nabla^2/(2\mu) + V(\vec{\mathbf{R}})$ , where  $\mu = m/2$  and  $m$  is the mass of the Er or Tm atom [35]. We discretize the radial component of the kinetic energy operator  $-\hbar^2\nabla^2/(2\mu)$  using the discrete-variable representation of Ref. [36]. Details regarding the selection of the spin and angular momentum basis and, in particular, the orbital or partial-wave angular momentum  $\vec{\ell}$  and total molecular angular momentum  $\vec{J}$  of the two rotating atoms are given in Sec.. We present results from two calculations. One is based on potential  $V(\vec{\mathbf{R}})$  including only the two dominant spin tensors  $\hat{T}_0^{(1)}$  and  $\hat{T}_2^{(1)}$ , constructed by joining the electronic structure data with the long-range potentials, and one where all seven tensor operators are included. For latter case, the  $R$ -dependence of the remaining five weaker spin tensor operators is given by their long-range form for all  $R$ .

Figure 4 shows three views of ro-vibrational eigenenergies of bosonic  $^{168}\text{Er}_2$  states near the minimum of the adiabatic potentials. As the nuclear spin of  $^{168}\text{Er}$  is zero *gerade* basis states have even values for partial wave  $\ell$ . *Ungerade* basis states require odd  $\ell$ . The pattern of the energy levels in the  $hc \times 150 \text{ cm}^{-1}$  energy range in Fig. 4a) can be understood from the seven  $0_g^+$  adiabatic potentials shown in Figs. 2a) and b) and Eq. (9). The vibrational energy spacing based on the harmonic approximation around the minima of the nearly-parallel adiabatic potentials is  $hc \times 27.0 \text{ cm}^{-1}$  so that vibrational levels  $v = 0, 1, \dots, 5$  are visible in the figure. For each  $v$  the spacings among the seven  $0_g^+$  states are to good approximation found from  $\sqrt{6}V_{k=2}^{(1)}(R_e)\Omega_1^2$  for  $|\Omega_1| = 0, \dots, 6$  with  $\sqrt{6}V_{k=2}^{(1)}(R_e) = hc \times 2.3 \text{ cm}^{-1}$  at the equilibrium separation. The  $\Omega_1$  fine-structure thus overlaps with the vibrational structure.

Figure 4b) shows  $v = 0$   $\Omega_{g/u}^\pm$   $^{168}\text{Er}_2$  eigenstates over an energy region of only  $hc \times 15 \text{ cm}^{-1}$  versus total molecular angular momentum  $J$ . based on calculations that include all spin tensors. Panel c) shows equivalent data including only the two strongest spin tensors. The level density in both two panels is large, although the level patterns are distinct with differences around  $hc \times 1 \text{ cm}^{-1}$ . In other words, the weaker spin-tensors can not be ignored in an accurate analysis of the lowest energy states of  $\text{Er}_2$ .

Surprisingly, we predict that the  $J = 10$  rotational state of the  $v = 0$   $0_g^+$  ground state has the absolute lowest energy when all interactions are included. The reason for this and other unexpected rotational progressions is the degeneracies of different  $\Omega$  states inherent in the model of Eq. (9) as well as more accidental degeneracies due to the high level density. The coriolis force in a rotat-

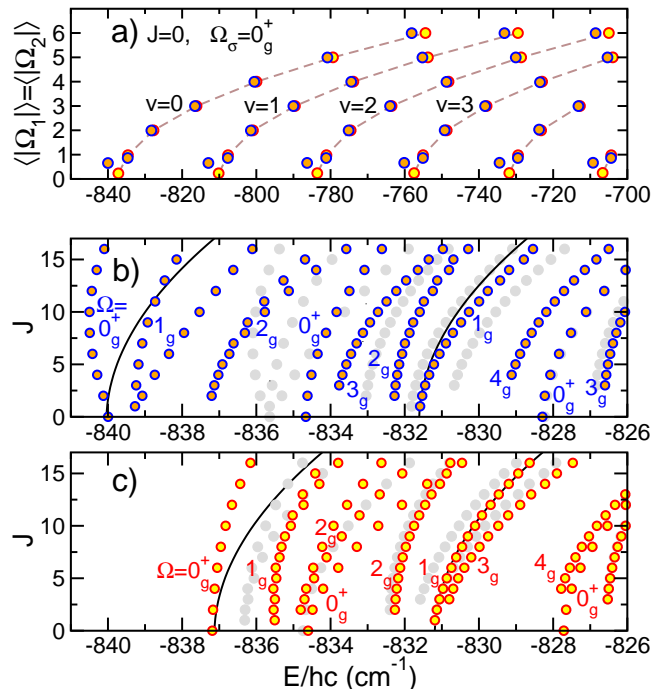


FIG. 4. Three views of eigenenergies  $E$  of bosonic  $^{168}\text{Er}_2$  near the minima of its potentials. Energies are with respect to the dissociation limit of two  $^{168}\text{Er}$  atoms. Panel a) shows the energies of the fine-structure components for the six energetically-lowest  $J = 0$  vibrational levels  $v$  of the  $0_g^+$  state. For each  $v$  these  $0_g^+$  states are uniquely labeled by the expectation value of  $|\Omega_1|$ , which are close to integer valued. Orange-filled and yellow-filled circles are the result of calculations that include all spin-tensor interactions and only include the two strongest spin tensors, respectively. Panels b) shows the energies of  $v = 0$  rotational eigenstates versus  $J$  for calculations that include all tensor operators, while panel c) shows equivalent data including only the two strongest spin tensors. Labeled colored circles correspond to *gerade* states. Solid gray markers correspond to the energies of *ungerade* states. Finally, black curves in panels b) and c) correspond to progressions  $B_e J(J+1)$ , where  $B_e = hc \times 0.0095 \text{ cm}^{-1}$  is the rotational constant at the equilibrium separation.

ing molecule breaks these (near-)degeneracies for states with  $\Omega$  values that differ by one unit. For large  $J$  coupling matrix elements are on the order of  $B_e J j_1$ , which can easily reach values of order  $hc \times 1 \text{ cm}^{-1}$  comparable to or larger than  $V_{k=2}^{(1)}(R_e)$ , even when  $B_e$  is not. Degenerate perturbation theory then predicts “rotational” progressions of the form  $\pm A_e J + B_e J(J+1)$ , where energy  $A_e$  with  $|A_e| \gg B_e$  can be computed on a case basis.

Figure 5 shows the lowest eigenenergies of  $^{169}\text{Tm}_2$  near the minimum of its adiabatic potentials versus total molecular angular momentum  $J$ . Both *gerade* and *ungerade* states are shown and assigned  $\Omega_{g/u}^\pm$  labels. The nuclear spin  $\vec{i}$  of  $^{169}\text{Tm}$  is  $1/2$ , making the atoms bosons, and hyperfine interactions of the form  $a_{\text{hf}} \vec{j}_1 \cdot \vec{i}_1 / \hbar^2$  etc.

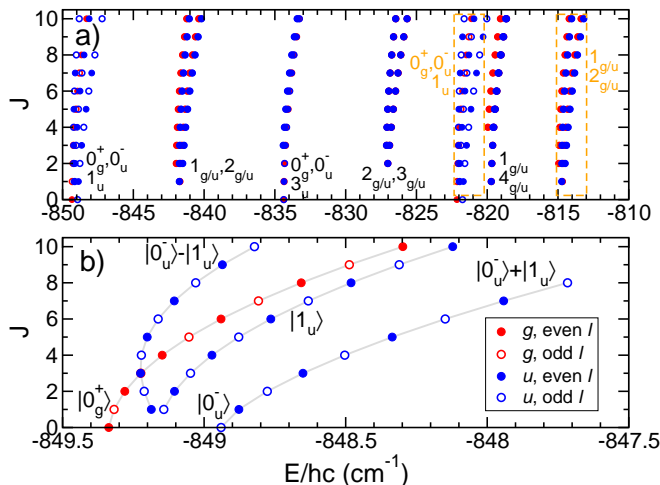


FIG. 5. Eigenenergies  $E$  of  $^{169}\text{Tm}_2$  near the minima of its potentials. Energies are with respect to the dissociation limit of two  $^{169}\text{Tm}$  atoms. Panel a) shows energies of  $v = 0$  and  $v = 1$   $\Omega_\sigma^\pm$  vibrational and fine-structure eigenstates versus total molecular angular momentum  $J$  for calculations that include all spin-tensors interactions. Levels enclosed by orange dashed boxes are  $v = 1$  states. All others are  $v = 0$  states. Panel b) shows a blowup of the energies of the energetically-lowest  $0_g^+$ ,  $0_u^-$ , and  $1_u$  states. Unusual rotational progressions are visible and are discussed in the text. Color and type of markers, as indicated in the legend box, separate *gerade* from *ungerade* states as well as even from odd partial wave  $\ell$  states and are the same in both panels.

mix *gerade* and *ungerade* states, although even and odd  $\ell$  remain uncoupled. We do not include such interactions and *gerade* states with either even and odd  $\ell$  must be shown. Similarly, *ungerade* states with even and odd  $\ell$  exist. It is worth noting that the  $^{169}\text{Tm}$  hyperfine constant  $a_{\text{hf}} = hc \times 0.0062 \text{ cm}^{-1}$  [16] and hyperfine couplings can mostly be neglected in the analysis of the bound states on the scale shown in the figure.

The  $\text{Tm}_2$  level structure is significantly simpler than that for  $\text{Er}_2$ , even though the vibrational spacings and rotational constants of the two dimers are nearly the same. The dominant anisotropic spin-tensor interaction in  $\text{Tm}_2$  is close to three times larger than in  $\text{Er}_2$ , as seen in Fig. 3, thereby reducing the number of  $\Omega_\sigma^\pm$  states between the  $v = 0$  and 1 vibrational states. The vibrational and rotational spectroscopic constants for  $\text{Tm}_2$  are  $hc \times 27.2 \text{ cm}^{-1}$  and  $hc \times 0.0096 \text{ cm}^{-1}$ , respectively. Unlike for  $\text{Er}_2$  the remaining five weaker spin-tensor operator play no significant role.

Figure 5b) shows that the  $v = 0$ ,  $J = 0$   $0_g^+$  state is the absolute ground state. This  $0_g^+$  state has a “simple”  $B_e J(J + 1)$  rotational progression. The nearby *ungerade* states have a less-conventional rotational progression. Here, this follows from the *four-fold* degeneracy for the lowest-energy states implied by Eq. (9). The four states have  $|\Omega_1| = |\Omega_2| = 1/2$  and labels  $\Omega_\sigma^\pm = 0_g^+$ ,  $0_u^-$  and twice  $1_u$ . In fact, a careful analytical analysis of the cen-

trifugal and coriolis interactions within the degenerate manifold shows that in the limit  $J \rightarrow 0$  the *ungerade* levels have energies that lie tens of  $B_e$  above that of the  $0_g^+$  state. For large  $J$  two of the three *ungerade* states become equal mixtures of  $1_u$  and  $0_u^-$ . The *ungerade* state with the second-lowest energy remains of pure  $1_u$  symmetry. Finally, we observe that the energetically-lowest *ungerade* state has  $J = 3$ .

### III. METHODS

#### A. Spin-stretched electronic potentials.

The spin-stretched potentials  $V_{\text{ss}}(R)$  for  $\text{Er}_2$  and  $\text{Tm}_2$  have been obtained from (partially-) spin-restricted single-reference non-relativistic coupled-cluster calculations that included single, double and perturbative triple (RCCSD(T)) excitations [37]. For the calculations the total electron spin  $S$  is 2 and 1 for  $\text{Er}_2$  and  $\text{Tm}_2$ , respectively. In addition, the projection quantum number  $\Lambda$  of the total electron orbital angular momentum along the internuclear axis is 10 and 6 for  $\text{Er}_2$  and  $\text{Tm}_2$ , respectively.

We use the Stuttgart/Cologne “small-core” quasi-relativistic effective core potentials (ECPs) developed for rare-earth elements (ECP28MWBSO)[38] to describe the twenty eight 1s, 2sp, and 3spd electrons of the Er and Tm atoms. The remaining electrons are described by the Relativistic Small Core Segmented (RSCSEG)[39] atomic basis set of quadruple-zeta quality developed for the ECPs. We extend the basis set with three diffuse Gaussian s functions with exponents 0.1495, 0.01, and 0.00412; two p functions with exponents 0.04895 and 0.0211; one d function with exponent 0.02799; and one f and g function both with exponent 0.1068, respectively. All exponents are in units of  $a_0^{-2}$ . In order to converge the preliminary self-consistent-field (SCF) calculations of neutral  $\text{Er}_2$  and  $\text{Tm}_2$ , we start from the SCF orbitals for molecular ions  $\text{Er}_2^{4+}$  and  $\text{Tm}_2^{4+}$ .

Based on a comparison of results found with different basis set size, the one-standard-deviation uncertainty of the spin-stretched potential is about  $hc \times 50 \text{ cm}^{-1}$  at the equilibrium separation and drops to less than  $hc \times 1 \text{ cm}^{-1}$  at  $R = 20a_0$ . See tables in the Appendices for precise data on the spin-stretched potentials. A description of the extrapolation to  $R > 20a_0$  can also be found there.

#### B. Relativistic calculation of potential splittings.

We use the direct relativistic configuration interaction (DIRRCI) method [40] in DIRAC [29] to determine the energy splittings between the relativistic adiabatic potential curves of  $\text{Er}_2$  and  $\text{Tm}_2$  dissociating to two ground-state atoms.

As in the non-relativistic calculations converging SCF calculations for the neutral dimers start from SCF or-

bitals for  $\text{Er}_2^{4+}$  and  $\text{Tm}_2^{4+}$ . A reordering of the occupied 6s and open-shell 4f orbitals is then required in the input data for DIRAC. In practice, we only determine the SCF orbitals at  $R = 12a_0$  in this manner. SCF orbitals for  $R < 12a_0$  are found starting from orbitals for the neutral dimer obtained for a slightly larger  $R$ . We repeat the scheme to small  $R$  until the potentials are repulsive.

The active space in the DIRRCI calculations is solely composed of molecular orbitals arising from the 4f atomic shells. The 6s orbitals are kept doubly occupied and are not part of the active space. In addition, 5d orbitals remain unoccupied. These constraints balance the need for reasonable estimates of splittings among the relativistic potentials and a reasonable run-time and memory usage for the calculations. For state assignment it proved useful to determine the expectation values of the  $z$ -components of the total electronic orbital angular momentum and spin operators along the internuclear axis.

DIRRCI calculations have been performed for 25 and 28 internuclear separations between  $7a_0 < R \leq 12a_0$  for  $\text{Er}_2$  and  $\text{Tm}_2$ , respectively. At each of these  $R$  values, we determine the 91 relativistic potential energies and eigenstates for  $\text{Er}_2$ . For  $\text{Tm}_2$  we find 36 eigenpairs. An eigenstate is uniquely labeled by  $n, \Omega_{g/u}^\pm$  with  $n = 1, 2, 3, \dots$  for  $\Omega_{g/u}^\pm$  states ordered by increasing potential energy. We denote relativistic eigenenergies by  $U_{\text{rel}}(R; n, \Omega_{g/u}^\pm)$ . For the  $12_g$  and  $7_u$  spin-stretched state for  $\text{Er}_2$  and  $\text{Tm}_2$ , respectively, there exists just one potential dissociating to two ground state atoms. For our identical ground-state atoms *gerade* states are  $0^+$  states, while *ungerade* states are  $0^-$  states. A discussion of di-atomic symmetries and molecular state labels can be found in Refs. [41] and [42].

With the constraints on the active space in the DIRRCI calculations, we sacrificed on the accuracy of the depth of the potentials. Those are mainly determined by excitations of electrons out of the 6s orbitals. In order to obtain accurate adiabatic potential energy curves  $V_{\text{rel}}(R; n, \Omega_{g/u}^\pm)$ , we assume that the non-relativistic spin-stretched potential  $V_{\text{ss}}(R)$  is a good representation of the potential for the relativistic spin-stretched state. The adiabatic potentials for the other adiabatic states are then

$$V_{\text{rel}}(R; n, \Omega_{g/u}^\pm) = V_{\text{ss}}(R) - \left( U_{\text{rel}}(R; n, \Omega_{g/u}^\pm) - U_{\text{rel}}(R; 1, \Omega_{\text{ss}}) \right) \quad (13)$$

when  $R \leq 12a_0$  and  $\Omega_{\text{ss}} = 12_g$  and  $7_u$  for  $\text{Er}_2$  and  $\text{Tm}_2$ , respectively. The uncertainties in the  $R \leq 12a_0$  calculations and extrapolation to  $R > 12a_0$  using the long-range dispersion potentials are discussed in the Appendices. The potentials in Eq. (13) are used in the least-squares fitting to spin-tensor operators as described in the main text.

### C. Basis sets in ro-vibrational state calculations.

We use the unit-normalized coupled spin and angular momentum basis

$$|(j_{\text{el}}\ell)JM\rangle \equiv \sum_{m_j m_\ell} |(j_1 j_2)j_{\text{el}} m_{\text{el}}\rangle Y_{\ell m_\ell}(\hat{\mathbf{R}}) \langle j_{\text{el}} \ell m_{\text{el}} m_\ell | JM \rangle \quad (14)$$

for the calculation of ro-vibrational states of  $\text{Er}_2$  and  $\text{Tm}_2$  with

$$|(j_1 j_2)j_{\text{el}} m_{\text{el}}\rangle = \sum_{m_1 m_2} |j_1 m_1\rangle |j_2 m_2\rangle \langle j_1 j_2 m_1 m_2 | j_{\text{el}} m_{\text{el}}\rangle$$

and spherical harmonic functions  $Y_{\ell m}(\hat{\mathbf{R}})$ . Here,  $\langle j_1 j_2 m_1 m_2 | j m \rangle$  are Clebsch-Gordan coefficients. The total molecular angular momentum  $\vec{J} = \vec{\ell} + \vec{j}_{\text{el}}$  is conserved,  $\vec{j}_{\text{el}} = \vec{j}_1 + \vec{j}_2$ , and projection quantum numbers  $m_x$  and  $M$  are with respect to a space-fixed coordinate system. Basis states with even and odd  $j_{\text{el}}$  contribute to *gerade* and *ungerade* molecular states, respectively, and are not mixed by the molecular Hamiltonian. Similarly, the Hamiltonian does not couple basis states with even partial wave  $\ell$  with those with odd  $\ell$ . Atomic masses have been taken from Refs. [43, 44] and atomic  $g$ -factors from Ref. [45].

## IV. CONCLUSIONS

We have studied the electronic properties of two heavy homonuclear lanthanide molecules,  $\text{Er}_2$  and  $\text{Tm}_2$ . A hybrid non-relativistic/relativistic electronic structure approach was needed to overcome the computational challenges arising from the complexity of their open submerged 4f electronic shell structure partially hidden by a closed  $6s^2$  shell. This allowed us for the first time to determine a complete set of ground-state potentials for a wide range of interatomic separations.

A non-relativistic coupled-cluster calculation was used to determine the spin-stretched potential energy surfaces with the maximum allowed total electron spin  $S$  and projection quantum number  $\Lambda$  of the total electron orbital angular momentum along the internuclear axis. Then we used a relativistic multi-configuration-interaction calculation to determine the splittings among the potentials dissociating to two ground state atoms. There are 91 *gerade/ungerade* potentials for  $\text{Er}_2$  (with  $\Omega$ s from 0 to 12) and 36 potentials for  $\text{Tm}_2$  (with  $\Omega$ s from 0 to 7). We identified the splittings as due to different relative orientations of the angular momenta of 4f shell electrons.

To facilitate the application of our electronic structure predictions in spectroscopic and scattering dynamics studies we analytically expressed the potential energy operator for  $\text{Er}_2$  and  $\text{Tm}_2$  as a sum of a small number of spherical-tensor operators and elucidated the relationships between their electrostatic, relativistic, and magnetic dipole-dipole interactions. The most remark-

able aspect of this analysis is that to good approximation the potential energy operator can be described with only two spin-tensor interactions, one isotropic and one anisotropic.

Finally, we computed the spectroscopically relevant lowest ro-vibrational eigenstates of Er<sub>2</sub> and Tm<sub>2</sub>. This data can be used as preliminary information for setting up spectroscopic studies of these exotic and technologically important systems.

## Acknowledgements

Work at Temple University is supported by the U.S. Air Force Office of Scientific Research Grant #FA9550-21-1-0153, the Army Research Office Grant #W911NF-17-1-0563, and the NSF Grant #PHY-1908634.

## Data availability statement

The data in this paper is self contained.

## Appendix A: Table of content for Appendices

These appendices contain the input data and a derivation needed to reproduce the potentials presented in our article on the interactions between two ground-state erbium atoms and two ground-state thulium atoms. We give tables for non-relativistic spin-stretched potentials and relativistic anisotropic spin-tensor strengths. The main text has a graph of the potentials of *gerade* states of the two dimers. Here, we present the equivalent figure of potentials for *ungerade* states.

In addition, we derive the long-range van-der-Waals dispersion interactions for our high-spin Er and Tm atoms. We find that these interactions can be described in terms of seven spin-tensor operators, whose strengths or van-der-Waals coefficients are linearly dependent. In fact, only four independent dispersion coefficients exist. We also give tables of Er and Tm atomic transition frequencies and Einstein *A* coefficients or oscillator strengths on which the values of the dispersion coefficients in the table in the main text are based.

We use Planck's constant  $h$  and the speed of light in vacuum  $c$  in converting energies into wavenumbers.

## Appendix B: Non-relativistic spin-stretched states of Er<sub>2</sub> and Tm<sub>2</sub>

The spin-stretched potentials for Er<sub>2</sub> and Tm<sub>2</sub> dissociating to two ground-state atoms have been obtained from non-relativistic single-reference coupled-cluster calculations that included single, double and perturbative triple excitations (RCCSD(T)). The orbital basis sets for these calculations have been described in Sec. III. The total electron spin  $S$  and orbital-angular-momentum projection quantum number  $\Lambda$  are conserved quantities and for this state have their maximum allowed value. We have  $(S, \Lambda) = (2, 10)$  and  $(1, 6)$  for Er<sub>2</sub> and Tm<sub>2</sub>, respectively.

The spin-stretched potential  $U_{ss}(R)$  for Er<sub>2</sub> has been determined with coupled-cluster theory as implemented in CFOUR [46] at 59 separations between  $R_{\min} = 7.3a_0$  and  $R_{\max} = 20a_0$  as well as at  $R_{\infty} = 200a_0$  in order to determine the dissociation energy of the potential. Here,  $a_0 = 0.0529177$  nm is the Bohr radius. The spin-stretched potential for Tm<sub>2</sub> has been determined using coupled-cluster theory as implemented in Molpro [47] at 72 separations between  $R_{\min} = 6.25a_0$  and  $R_{\max} = 20a_0$  as well as at  $R_{\infty} = 60a_0$ . Potentials

$$V_{ss}(R) = U_{ss}(R) - U_{ss}(R_{\infty}) \quad (\text{B1})$$

of Er<sub>2</sub> and Tm<sub>2</sub> up to  $R = R_{\max}$  are given in Tables II and III, respectively.

The spin-stretched potential for  $R < R_{\min}$  is found by linear extrapolation using the first two separations larger than or equal to  $R_{\min}$ . For  $R > R_{\text{disp}}$  with  $R_{\text{disp}} > R_{\max}$  we use the dispersive form

$$V_{\text{disp}}(R) = C_{6,ss}/R^6 + C_{8,ss}/R^8 + C_{10,ss}/R^{10}, \quad (\text{B2})$$

where the van-der-Waals coefficient  $C_{6,ss}$  is

$$C_{ss} = C_0^{(1)} + (2j)(2j-1)C_2^{(1)}/\sqrt{6} \quad (\text{B3})$$

with  $j = 6$  and  $7/2$  for Er<sub>2</sub> and Tm<sub>2</sub>, respectively based on two relevant values for  $C_k^{(i)}$  are given in the table in the main text and the derivation in this Appendix B. Coefficients  $C_{8,ss}$  and  $C_{10,ss}$  are fixed such that the dispersive form agrees with the potential energy from coupled-cluster theory at the two largest radial points  $R \leq R_{\max}$ . We use  $R_{\text{disp}} = R_{\max} + 0.5a_0$  for both Er<sub>2</sub> and Tm<sub>2</sub>, add  $(R_{\text{disp}}, V_{\text{disp}}(R_{\text{disp}}))$  to the coupled-cluster data, and for  $R \in (R_{\min}, R_{\text{disp}})$  interpolate this extended coupled-cluster data set times  $R^6$  using the Akima spline [48]. The function  $R^6 V_{ss}(R)$  varies significantly less than  $V_{ss}(R)$ . The fitted  $C_{8,ss}$  are consistent with typical values based on the induced quadrupole-quadrupole interaction for other di-atomic molecules [49] and the contributions from the five omitted dispersion terms is small compared to the uncertainties in the potentials.

The uncertainty budget of  $V_{ss}(R)$  as function of  $R$  has two components. The first is the complete basis set error of the RCCSD(T) calculations. The second is that four-electron excitations might need to be included in our open-shell molecules. This corresponds to accounting for non-perturbative triple as well as quadruple excitations. Basis-set superpositions errors increase the depth of the potentials  $V_{ss}(R)$ , while non-perturbative triple and quadruple corrections often are of opposite sign, nearly cancel, but lead to shallower potentials for dimers [50, 51]. Here, based on the differences of calculations with triple- and quadruple-zeta accuracy basis sets, we assume that the one-standard-deviation uncertainties of  $V_{ss}(R)$  is  $2 \times u(C_0^{(1)})/R^6$  for  $R < R_{\max}$ , where  $u(C_0^{(1)})$  is the one-standard-deviation uncertainty of the isotropic dispersion coefficient  $C_0^{(1)}$ .

TABLE II. Potential energy  $V_{ss}(R)$  of the energetically-lowest “spin-stretched” state of  $\text{Er}_2$   $\Omega=12_g$  as function of internuclear separation  $R$ . The  $R$ -dependent uncertainty of this potential is discussed in the text.

$R/a_0$	$V_{ss}/hc$ ( $\text{cm}^{-1}$ )	$R/a_0$	$V_{ss}/hc$ ( $\text{cm}^{-1}$ )	$R/a_0$	$V_{ss}/hc$ ( $\text{cm}^{-1}$ )
7.3	136.928967055564	9.3	-702.972094884141	11.6	-290.170412396272
7.4	-33.4063015426345	9.4	-685.377674371753	11.8	-265.152758759965
7.5	-179.030466142739	9.5	-666.764780470275	12.2	-221.189686201221
7.6	-302.624146371783	9.6	-647.392883509601	12.6	-184.510652309416
7.7	-406.626745855377	9.7	-627.480644193817	13.0	-154.076250986245
7.8	-493.261808207445	9.8	-607.236006360562	13.5	-123.313365467909
7.9	-564.543330776862	9.9	-586.808634364519	14.0	-99.0517088984615
8.0	-622.296924164693	10.0	-566.344786996666	14.5	-79.8868022335593
8.1	-668.163414255055	10.1	-545.963873169331	15.0	-64.7056634495449
8.2	-703.629551622843	10.2	-525.767267986650	15.5	-52.6401140333373
8.3	-730.026393137440	10.3	-505.840657675087	16.0	-43.0174850895937
8.4	-748.547347148735	10.4	-486.253895514174	16.5	-35.3133121226139
8.5	-760.256868094275	10.5	-467.064631313888	17.0	-29.1215244271569
8.6	-766.106999612316	10.6	-448.319777407923	17.5	-24.1273429014569
8.7	-766.942290212839	10.7	-430.056805726134	18.0	-20.0834953954821
8.8	-763.511447018345	10.8	-412.304806381708	18.5	-16.7958394274081
8.9	-756.477032518151	10.9	-395.085506635547	19.0	-14.1139773714497
9.0	-746.423038708948	11.0	-378.414408279889	19.5	-11.9094506999236
9.1	-733.862648819818	11.2	-346.752289713281	20.0	-10.0943440302398
9.2	-719.246967350335	11.4	-317.346954936712		

TABLE III. Potential energy  $V_{ss}(R)$  of the energetically-lowest “spin-stretched” state of  $\text{Tm}_2$  as function of internuclear separation  $R$ . The  $R$ -dependent uncertainty of this potential is discussed in the text.

$R/a_0$	$V_{ss}/hc$ ( $\text{cm}^{-1}$ )	$R/a_0$	$V_{ss}/hc$ ( $\text{cm}^{-1}$ )	$R/a_0$	$V_{ss}/hc$ ( $\text{cm}^{-1}$ )
6.25	3874.15018867483	8.6	-775.049924968957	10.75	-409.392022314815
6.5	2452.88195449737	8.7	-772.46879342323	11.0	-367.345465164348
6.75	1398.48143296268	8.75	-769.709228982994	11.25	-328.942955195758
6.8	1224.59520643307	8.8	-766.073434020327	11.5	-294.175889173847
6.9	909.16853126916	8.9	-756.484235631714	11.75	-262.878651327859
7.0	633.431409261034	9.0	-744.222911614132	12.0	-234.883475377653
7.1	393.453268965899	9.1	-729.769650342498	12.25	-209.924884847286
7.2	185.614885631341	9.2	-713.532718742361	12.5	-187.720788736913
7.25	92.6843395024816	9.25	-704.864106741569	12.75	-168.003713562084
7.3	6.56791035932326	9.3	-695.884191964824	13.0	-150.499513340797
7.4	-146.706530584091	9.4	-677.132015128778	13.5	-121.195083284982
7.5	-276.986305870368	9.5	-657.551518907663	14.0	-98.0218311326522
7.6	-386.841551372091	9.6	-637.379384988748	14.5	-79.6165119880272
7.7	-478.589634023197	9.7	-616.821173105488	15.0	-64.9113377098249
7.75	-518.306204431474	9.75	-606.45387137768	15.5	-53.1237496407613
7.8	-554.273972390536	9.8	-596.054548248776	16.0	-43.6507851515064
7.9	-615.850590443533	9.9	-575.229126068204	16.5	-36.0202004857629
8.0	-664.991862988103	10.0	-554.467856276277	17.0	-29.8546529570767
8.1	-703.262622294269	10.1	-533.883746459349	17.5	-24.8547571665504
8.2	-732.03585776905	10.2	-513.570051395331	18.0	-20.7752063343089
8.25	-743.254940662834	10.25	-503.537338666485	18.5	-17.4646289323737
8.3	-752.551798724083	10.3	-493.597463728117	19.0	-14.7468524614891
8.4	-765.919099466286	10.4	-474.031826052711	19.5	-12.5153879327555
8.5	-773.126032186692	10.5	-454.926141284319	20.0	-10.664119330474

### Appendix C: Relativistic configuration-interaction calculations and expansion in spin tensor operators

We have used the direct relativistic configuration interaction (DIRRCI) method in DIRAC 2019 [29] to determine the energy splittings among the relativistic adiabatic potential curves of  $\text{Er}_2$  and  $\text{Tm}_2$  for  $R \leq 12a_0$ .

Basis sets have been described in Sec. ???. In Sec. ??, we also described how the spin-stretched potential  $V_{ss}(R)$  and the energy splittings are used to construct relativistic adiabatic potential curves  $V_{\text{rel}}(R; n, \Omega_{g/u}^{\pm})$ . We find a common uncorrelated one-standard-deviation uncertainty  $u(R) = hc \times 10 \text{ cm}^{-1}$  independent of  $R$  for all potential energy splittings. This follows from a compar-

ison of DIRRCI calculations with different basis set size. In addition, the uncertainty in the splittings and that of  $V_{ss}(R)$  are uncorrelated.

The  $V_{\text{rel}}(R; n, \Omega_{g/u}^{\pm})$  were fit to an expansion in terms of seven spin-spin tensor operators with strengths  $V_k^{(i)}(R)$  defined in the main text. Only  $V_0^{(1)}(R)$  and  $V_2^{(1)}(R)$  were found to be statistically relevant and we finally decided to only present results with those two strengths as fitting parameters with the remaining five strengths set to zero. The reduced chi-square  $\chi_{\nu}^2$  of this adjustment is less than one for all  $R < 12a_0$  so that the fit is consistent.

Tables IV and V contain values of the spin tensor strengths  $V_0^{(1)}(R)$  and  $V_2^{(1)}(R)$  as functions of interatomic separations for  $\text{Er}_2$  and  $\text{Tm}_2$ , respectively. Note that as the uncertainty in the splittings and that of  $V_{ss}(R)$  are uncorrelated strictly speaking strength  $V_2^{(1)}(R)$  is the only adjusted constant and

$$V_0^{(1)}(R) = V_{ss}(R) - (2j)(2j-1)V_2^{(1)}(R)/\sqrt{6}, \quad (\text{C1})$$

where  $j = 6$  and  $7/2$  for  $\text{Er}_2$  and  $\text{Tm}_2$ , respectively. The spin-tensor strength  $V_2^{(1)}(R)$  has an one-standard-deviation uncertainty of  $hc \times 0.094 \text{ cm}^{-1}$  and  $hc \times 0.40 \text{ cm}^{-1}$  for  $\text{Er}_2$  and  $\text{Tm}_2$  independent of  $R$ , respectively. The uncertainty of  $V_0^{(1)}(R)$  follows from error propagation of Eq. (C1). The contribution from  $V_{ss}(R)$  always dominates. In addition, the absolute value of the difference between  $V_0^{(1)}(R)$  and  $V_{ss}(R)$  are no larger than the uncertainty of  $V_{ss}(R)$  for all  $R$ . Hence, we surmise that the relativistic corrections to the non-relativistic spin-stretched potential  $V_{ss}(R)$  are of similar magnitude as well.

For  $R > 12a_0$  the relativistic configuration-interaction calculations do not converge. As shown in Fig. 4 in the main text, however, the adjusted anisotropic strengths  $V_2^{(1)}(R)$  at  $R = 12a_0$  for the two dimers are already consistent, *i.e.* within our uncertainties, with its asymptotic van-der-Waals  $C_2^{(1)}/R^6$  behavior. We then use the van-der-Waals behavior for  $R > R_{\text{rel}}$  with  $R_{\text{rel}} = 12a_0 + 0.5a_0$ . A smooth connection of the strength between  $12a_0$  and  $R_{\text{rel}}$  is ensured by adding point  $(R_{\text{rel}}, C_2^{(1)}/R_{\text{rel}}^6)$  to the  $R \leq 12a_0$  fitted values for  $V_2^{(1)}(R)$  and interpolate  $R^6 V_2^{(1)}(R)$  with the Akima spline [48].

Finally, even though the five weaker  $V_k^{(i)}(R)$  are consistent with zero in the least-squares adjustment, we use  $V_k^{(i)}(R) = C_k^{(i)}/R^6$  for all  $R$  for these five strengths in the calculation of the rovibrational levels of  $\text{Er}_2$  and  $\text{Tm}_2$ .

Figure 6 shows the *ungerade* potentials of  $\text{Er}_2$  and  $\text{Tm}_2$  near their equilibrium separation. The figure complements the figure with *gerade* state potentials in the main text

TABLE IV. Spin tensor strengths  $V_0^{(1)}(R)$  and  $V_2^{(1)}(R)$  for  $\text{Er}_2$  as functions of separation  $R$  for  $R \leq 12a_0$ . The isotropic strength  $V_0^{(1)}(R)$  is found from Eq. (C1). Its  $R$ -dependent uncertainty equals that of the potential of the spin-stretched state. The uncertainty of  $V_2^{(1)}(R)$  is  $hc \times 0.094 \text{ cm}^{-1}$  independent of  $R$ .

$R/a_0$	$V_0^{(1)}/hc$ ( $\text{cm}^{-1}$ )	$V_2^{(1)}/hc$ ( $\text{cm}^{-1}$ )
7.2		0.75334948
7.4	-86.14282611	0.97861800
7.6	-362.33159884	1.10797570
7.8	-555.79268757	1.16036930
8.0	-684.70138046	1.15802330
8.2	-763.82004690	1.11693940
8.4	-805.15566699	1.05046590
8.6	-818.30347406	0.96859643
8.8	-810.88531912	0.87910465
9.0	-788.86447184	0.78757466
9.2	-756.85758280	0.69793043
9.4	-718.37785998	0.61237588
9.6	-676.09538548	0.53262488
9.8	-632.01638040	0.45984297
10.0	-587.59296366	0.39429690
10.2	-543.84435218	0.33545176
10.4	-501.52123195	0.28331200
10.6	-461.13522634	0.23781296
10.8	-423.00143547	0.19849457
11.0	-387.29369989	0.16477071
11.2	-354.08026901	0.13598341
11.4	-323.36078965	0.11159717
11.6	-295.07053724	0.09093034
11.8	-269.11169606	0.07346497
12.0		0.05871469

#### Appendix D: Derivation of the dispersion potentials

Long-range van-der-Waals dispersion interactions have been derived and studied in many settings [34, 52, 53]. We repeat part of these derivations in order to explain the relationships among the strengths of the seven spin-tensor operators contributing the atom-atom interaction  $V(\mathbf{R})$  for large separations  $R$ . In this section we rely on Ref. [32] for notation regarding angular momentum operators as well as the manipulation of these operators with one clearly-stated exception regarding reduced matrix elements.

We consider interacting atoms with electronic eigenstates  $|n b \beta\rangle$  with total electronic angular momentum quantum numbers  $b$ , projection quantum numbers  $\beta$  on a space- or laboratory-fixed axis, and energies  $E_{nb}$  that are independent of  $\beta$ . Label  $n$  further uniquely specifies states. The ground state of the atoms is  $|g j m\rangle$ .

The van-der-Waals potential operator between two ground-state atoms,  $|g_1 j_1 m_1, g_2 j_2 m_2\rangle = |g_1 j_1 m_1\rangle |g_2 j_2 m_2\rangle$ , is derived from (degenerate) second-order perturbation theory in the anisotropic electric

TABLE V. Spin tensor strengths  $V_0^{(1)}(R)$  and  $V_2^{(1)}(R)$  for  $\text{Tm}_2$  as functions of separation  $R$  for  $R \leq 12a_0$ . The isotropic strength  $V_0^{(1)}(R)$  is found from Eq. (C1). Its  $R$ -dependent uncertainty equals that of the potential of the spin-stretched state. The uncertainty of  $V_2^{(1)}(R)$  is  $hc \times 0.40 \text{ cm}^{-1}$  independent of  $R$ .

$R/a_0$	$V_0^{(1)}/hc$ ( $\text{cm}^{-1}$ )	$V_2^{(1)}/hc$ ( $\text{cm}^{-1}$ )
7.0	594.90655204	2.2468153
7.2	133.54032587	3.0370500
7.4	-206.86711784	3.5086367
7.6	-450.80090236	3.7301851
7.8	-618.71806662	3.7584559
8.0	-727.59730629	3.6512236
8.1	-764.32796312	3.5614030
8.2	-791.25843938	3.4539311
8.3	-809.69858744	3.3328684
8.4	-820.81468219	3.2015754
8.5	-825.64585040	3.0630180
8.6	-825.11351391	2.9197678
8.7	-820.03654142	2.7742074
8.8	-811.13357004	2.6279605
8.9	-799.04967438	2.4824668
9.0	-784.32927135	2.3390504
9.1	-767.46932713	2.1986898
9.2	-748.89238132	2.0622174
9.3	-728.98072835	1.9302292
9.4	-708.05036358	1.8031947
9.5	-686.38223486	1.6814415
9.6	-664.21695040	1.5651986
9.8	-619.19702752	1.3496968
10.0	-574.30698185	1.1570413
10.2	-530.48373364	0.98642598
10.4	-488.37811753	0.83669271
11.0	-375.85614024	0.49635265
12.0	-238.11360714	0.18838511

dipole-dipole interaction  $V_{\text{dd}}(\vec{\mathbf{R}})$  and is given by

$$V_{\text{vdW}}(\vec{\mathbf{R}}) = \sum'_{n_1 b_1 \beta_1, n_2 b_2 \beta_2} V_{\text{dd}}(\vec{\mathbf{R}}) |n_1 b_1 \beta_1, n_2 b_2 \beta_2\rangle \quad (\text{D1})$$

$$\times \frac{1}{E_{g_1 j_1} + E_{g_2 j_2} - E_{n_1 b_1} - E_{n_2 b_2}} \langle n_1 b_1 \beta_1, n_2 b_2 \beta_2 | V_{\text{dd}}(\vec{\mathbf{R}}),$$

where

$$V_{\text{dd}}(\vec{\mathbf{R}}) = -\frac{1}{4\pi\epsilon_0} \sqrt{6} \frac{1}{R^3} T_2(d_1, d_2) \cdot C_2(\hat{\mathbf{R}}), \quad (\text{D2})$$

$d_i$  is the rank-1 electric dipole moment operator of atom  $i = 1$  or  $2$ ,  $C_{kq}(\hat{\mathbf{R}})$  is a spherical harmonic, and rank- $k$  spherical-tensor operator  $T_{kq}(R, S) \equiv [R \otimes S]_{kq}$  with the  $\otimes$  notation of [31] is constructed from spherical-tensor operators  $R$  and  $S$  with rank  $r$  and  $s$ , respectively. The prime on the sums in Eq. (D1) indicates that the sums exclude the term where both atoms are in the ground state and  $b_i = |j_i - 1|, \dots, j_i + 1$ . The energy denominator is negative and does not depend on projection quantum numbers. Finally,  $\epsilon_0$  is the vacuum electric permittivity.

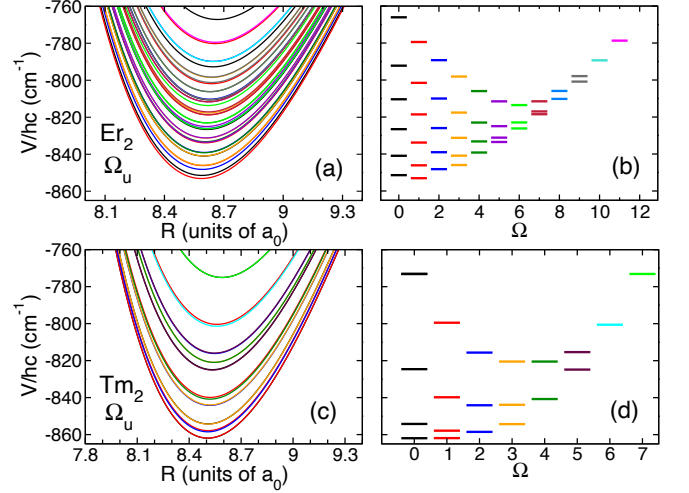


FIG. 6. Relativistic  $\Omega_u^\pm$  potential energy curves with *ungerade* symmetry for  $\text{Er}_2$  (panel a) and  $\text{Tm}_2$  (panel c) as functions of internuclear separation  $R$  near the equilibrium separation as obtained from electronic structure calculations. All potentials approach zero energy for  $R \rightarrow \infty$ . Panels (b) and (d) show potential energies from panels (a) and (c) using the same line colors at the equilibrium separation as functions of projection quantum number  $\Omega$  for  $\text{Er}_2$  and  $\text{Tm}_2$ , respectively. *Ungerade*  $\Omega = 0$  states are  $0^-$  states.

The sums in Eq. (D1) can be rearranged in several steps using Appendix VI of Ref. [32]. As operators  $d_1$  and  $d_2$  commute, we first note that

$$(T_2(d_1, d_2) \cdot C_2)(T_2(d_1, d_2) \cdot C_2) = \sum_k (-1)^k T_k(T_2(d_1, d_2), T_2(d_1, d_2)) \cdot T_k(C_2, C_2) \quad (\text{D3})$$

with  $T_{kq}(C_2, C_2) = \langle k0|2200\rangle C_{kq}$  and Clebsch-Gordan coefficient  $\langle j_3 m_3 | j_1 j_2 m_1 m_2 \rangle$ . We omitted the dependence on orientation  $\hat{\mathbf{R}}$  of the spherical harmonics for clarity. The right hand side of Eq. (D4) is only nonzero for even  $k = 0, 2$ , or  $4$ . Secondly, we note that

$$T_{kq}(T_2(d_1, d_2), T_2(d_1, d_2)) = 5 \sum_{l_1 l_2} \sqrt{(2l_1 + 1)(2l_2 + 1)} \times \begin{Bmatrix} 1 & 1 & l_1 \\ 1 & 1 & l_2 \\ 2 & 2 & k \end{Bmatrix} T_{kq}(T_{l_1}(d_1, d_1), T_{l_2}(d_2, d_2)), \quad (\text{D4})$$

where the  $d_i$  have been grouped by atom and  $l_i = 0, 1$ , or  $2$  and  $l_1 + l_2$  is even for a nonzero value of the nine- $j$  symbol  $\left\{ \begin{smallmatrix} \dots \\ \dots \end{smallmatrix} \right\}$ .

Next, we isolate the sums over projection quantum numbers and labels  $n$  in Eq. (D1). For atom  $i$ , we define spherical tensor operators

$$B_{lq}(b, j; i) = \sum_{\beta} T_{lq} \left( \frac{d_i |nb\beta\rangle}{\langle gj || d_i || nb\rangle}, \frac{\langle nb\beta | d_i}{\langle nb || d_i || gj\rangle} \right) \quad (\text{D5})$$

with rank  $l = 0, 1$ , or  $2$  and  $b = |j - 1|, \dots, j + 1$ . Here,  $\langle gj || d_i || nb\rangle$  and  $\langle nb || d_i || gj\rangle$  are reduced matrix elements

of the electric dipole moment operator between the atomic ground state and excited state  $|nb\beta\rangle$ . Crucially, for a ground-state atom we derive that

$$\langle gjm|B_{lq}(b, j; i)|gjm'\rangle = \langle jm|jlm'q\rangle\sqrt{(2b+1)(2l+1)}W(j1j1; bl) \quad (\text{D6})$$

based on the Wigner-Eckart theorem, Eq. (3.12) of Ref. [32], and symmetries of the Racah symbol  $W(abcd; ef)$ . These matrix elements are independent of label  $n$  of the excited state, but still depend on its total angular momentum  $b$ .

Moreover, using the Wigner-Eckart theorem again, we realize that the  $m, m'$ , and  $q$  dependences of  $\langle gjm|B_{lq}(b, j; i)|gjm'\rangle$  are identical to those for the identity operator, atomic angular momentum operator  $j_q$ , and dipole operator  $T_{2q}(j, j)$  for  $l = 0, 1$ , and  $2$ , respectively. In fact, we find

$$B_{lq}(b, j; i) = O_{lq}(i)M(b, j) \quad (\text{D7})$$

with rank- $l$  operator  $O_{lq}(i) = I, j_{iq}/\hbar$ , and  $T_{2q}(j_i, j_i)/\hbar^2$  for atom  $i$  and  $l = 0, 1$ , and  $2$ , respectively. Here,  $\hbar$  is the reduced Planck constant and the function  $M(b, j; l)$  is given by

$$M(b, j; l = 0) = (-1)^{b-j+1} \frac{1}{\sqrt{3}} \sqrt{\frac{2b+1}{2j+1}}, \quad (\text{D8})$$

$$M(b, j; l = 1) = \frac{(-1)^{b-j}}{2\sqrt{2}} \sqrt{\frac{2b+1}{2j+1}} \frac{2+j(j+1)-b(b+1)}{j(j+1)}, \quad (\text{D9})$$

and

$$M(b, j; l = 2) = \sqrt{\frac{2b+1}{2j+1}} \frac{W(j1j1; b2)}{W(j1j1; j2)} \frac{1}{j(j+1)}. \quad (\text{D10})$$

We put everything together to find for two ground-state atoms

$$\begin{aligned} V_{\text{vdW}}(\vec{\mathbf{R}}) &= \frac{1}{R^6} \sum_{k=0,2,4} \sum_{l_1 l_2} (T_k(O_{l_1}(1), O_{l_2}(2)) \cdot C_k(\hat{\mathbf{R}})) \\ &\times 30 \sqrt{\frac{(2l_1+1)(2l_2+1)}{(2j_1+1)(2j_2+1)}} \left\{ \begin{matrix} 1 & 1 & l_1 \\ 1 & 1 & l_2 \\ 2 & 2 & k \end{matrix} \right\} \langle k0|2200\rangle \\ &\times \sum_{b_1=|j_1-1|}^{j_1+1} \sum_{b_2=|j_2-1|}^{j_2+1} \frac{(-1)^{b_1-j_1} (-1)^{b_2-j_2}}{\sqrt{(2b_1+1)(2b_2+1)}} \quad (\text{D11}) \\ &\times M(b_1, j_1; l_1) M(b_2, j_2; l_2) h_{b_1 b_2}, \end{aligned}$$

where the matrix

$$h_{b_1 b_2} = \frac{1}{(4\pi\epsilon_0)^2} \sum_{n_1 n_2} \frac{(g_1 j_1 |d_1| |n_1 b_1)^2 (g_2 j_2 |d_2| |n_2 b_2)^2}{E_{g_1 j_1} + E_{g_2 j_2} - E_{n_1 b_1} - E_{n_2 b_2}} \quad (\text{D12})$$

or, equivalently,

$$E_h a_0^6 \sum_{n_1 n_2} \frac{(g_1 j_1 |d_1| |n_1 b_1)^2 (g_2 j_2 |d_2| |n_2 b_2)^2}{(E_{g_1 j_1} + E_{g_2 j_2} - E_{n_1 b_1} - E_{n_2 b_2})/E_h}$$

is symmetric for homonuclear dimers. Here,  $e$  is the elementary charge,  $E_h$  is the Hartree energy, and  $a_0$  is the Bohr radius. The prime in the sums over labels  $n_1$  and  $n_2$  excludes the case where both atoms are in their ground state and we have introduced the more symmetric reduced matrix elements  $(j||d||j') = (-1)^{j-j'} (j' ||d||j)^* = \sqrt{2j+1} \langle j||d||j'\rangle$  used by, for example, Edmonds in Ref. [54].

The allowed values for  $k, l_1$ , and  $l_2$  and the operators on the first line of Eq. (D11) lead to the seven spin-tensor operators defined in the main text. The last three lines of Eq. (D11) correspond to the van-der-Waals coefficients  $C_k^{(i)}$ . For example, the choice  $O_{l_1}(1) = j_1/\hbar$  and  $O_{l_2}(2) = j_2/\hbar$  leads to spin-tensor operators  $[j_1 \otimes j_2]_{k0}/\hbar^2$  with  $k = 0$  or  $2$  in the main text using the  $\otimes$  notation of Ref. [31] for combining spherical tensor operators. This notation is equivalent to the notation used in Ref. [32]. Further analysis of Eq. (D11) shows that the operators with the same  $l_1$  and  $l_2$  but different  $k$  have related van-der-Waals coefficients as the  $k$  dependence is isolated in the nine- $j$  symbol and the Clebsch-Gordan coefficient in the second line. This leads to the relationships between the two spin-tensors with  $l_1 = l_2 = 1$  and the three spin-tensors with  $l_1 = l_2 = 2$  given in the main text.

Lists of currently available atomic transition energies  $E_{nb} - E_{gj}$  and observed Einstein  $A$  coefficients or oscillator strengths  $f$  for erbium and thulium atoms are given in Tables VI, VII, and VIII below. The relevant relationships between the reduced matrix elements  $(gj||d||nb)$  in Eq. (D12) on the one hand and  $A$  and  $f$  on the other are

$$A_{nb \rightarrow gj} = \frac{4}{3} \frac{E_h}{\hbar} \alpha^3 \left( \frac{E_{nb} - E_{gj}}{E_h} \right)^3 \left| (gj || \frac{d}{ea_0} || nb) \right|^2 \frac{1}{2b+1} \quad (\text{D13})$$

and

$$f_{gj, nb} = \frac{2}{3} \frac{E_{nb} - E_{gj}}{E_h} \left| (gj || \frac{d}{ea_0} || nb) \right|^2 \frac{1}{2j+1}, \quad (\text{D14})$$

respectively. Here,  $\alpha$  is the fine-structure constant.

For  $\text{Er}_2$  atomic transition data or lines from 48 excited states to the ground state are available. The majority of the data is taken from Refs. [55, 56]. References [57] and [58] each supply one line, while for two other lines we rely on private communications [59, 60]. For  $\text{Tm}_2$  atomic transition data from 65 excited states to the ground state are available. Data have been taken from Refs. [45, 61, 62]. When line strength information of a transition is available from more than one source, the most accurate datum is chosen.

The uncertainties of and correlations among the van-der-Waals coefficients follow from error propagation on Eqs. (D11) and (D12) and are dominated by the uncorrelated uncertainties of the Einstein  $A$  coefficients and

oscillator strengths. Uncertainties in the transition energies give negligible contributions. Our values for the van-der-Waals coefficients are listed in the Table in the main text. Their covariances can be found in Table IX below.

TABLE VI. Atomic transition energies and Einstein  $A$  coefficients from excited states of erbium to its  $j' = 6$  ground state. Columns labeled  $\Delta E$ ,  $A$ ,  $u(A)$ , and  $j$  give transition energies, the value and one-standard deviation uncertainty of the Einstein  $A$  coefficients, and the total electronic angular momenta  $j$  of the excited states, respectively. A reference to the original data is given in columns labeled by “Ref.”.

$\Delta E/hc$ ( $\text{cm}^{-1}$ )	$A$ ( $10^6 \text{ s}^{-1}$ )	$u(A)$	$j$	Ref.	$\Delta E/hc$ ( $\text{cm}^{-1}$ )	$A$ ( $10^6 \text{ s}^{-1}$ )	$u(A)$	$j$	Ref.
11401.197	0.006377	0.00159425	5	[56]	23885.406	1.02	0.06	5	[55]
11799.778	0.01076	0.00269	6	[56]	24083.166	102.	5.	5	[55]
11887.503	0.01539	0.0038475	7	[56]	24457.139	32.6	1.6	6	[55]
15185.352	0.1431	0.035775	5	[56]	24943.272	220.	10.	7	[60]
15846.549	0.2624	0.0656	7	[56]	25159.143	40.3	2.1	7	[55]
16070.095	0.92	0.05	6	[55]	25162.553	37.6	1.9	5	[55]
16321.110	0.09051	0.0226275	6	[56]	25268.259	3.59	0.18	6	[55]
17073.800	0.24	0.06	6	[58]	25392.779	31.9	1.6	6	[55]
17157.307	1.17	0.06	7	[55]	25598.286	15.1	0.8	7	[55]
17347.860	0.84	0.04	5	[55]	25681.933	63.	3.	5	[55]
17456.383	0.1833	0.045825	6	[56]	25880.274	122.	6.	6	[55]
19201.343	0.53	0.053	5	[59]	26237.004	29.0	1.4	6	[55]
19326.598	0.663	0.16575	6	[56]	28026.045	0.59	0.05	5	[55]
19508.432	0.6392	0.1598	6	[56]	28053.943	4.33	0.22	6	[55]
21168.430	1.16	0.06	7	[55]	29550.807	0.064	0.007	5	[55]
21392.817	1.26	0.06	5	[55]	29794.862	0.296	0.025	5	[55]
21701.885	7.1	0.4	6	[55]	29894.203	4.10	0.29	5	[55]
22124.268	0.264	0.019	5	[55]	30007.369	7.7	1.93	6	[57]
22583.504	2.55	0.13	6	[55]	30251.891	1.05	0.08	5	[55]
22672.766	5.52	0.28	5	[55]	30380.282	4.3	0.3	5	[55]
23080.952	0.7405	0.185125	7	[56]	30600.160	0.168	0.017	5	[55]
23311.577	0.4924	0.1231	6	[56]	31442.927	0.084	0.009	5	[55]
23447.079	0.6011	0.150275	5	[56]	32062.166	0.175	0.027	5	[55]
23855.654	6.6	0.3	5	[55]	33485.216	9.6	0.7	5	[55]

TABLE VII. Some thulium excited atomic eigen energies with respect to its  $j' = 7/2$  ground state and oscillator strengths  $f$  from the ground state to these excited states. The first column gives the transition energy. The second and third column are the value and one-standard deviation uncertainty of the oscillator strength, respectively. The fourth column gives the total electronic angular momentum  $j$  of the excited state. A reference to the original data is given in the last column. Relevant thulium lines for which Einstein  $A$  coefficients are available can be found in Table VIII.

$\Delta E/hc$ ( $\text{cm}^{-1}$ )	$f$	$u(f)$	$j$	Ref.
38342.570	0.00169	0.00338	7/2	[62]
39019.090	0.00098	0.00196	9/2	[62]
39259.920	0.00262	0.00525	5/2	[62]
39580.720	0.00822	0.01644	7/2	[62]
39847.040	0.00192	0.00384	7/2	[62]
40101.720	0.00121	0.00242	9/2	[62]

TABLE VIII. Atomic transition energies and Einstein  $A$  coefficients from excited states of thulium to its  $j' = 7/2$  ground state. Columns labeled  $\Delta E$ ,  $A$ ,  $u(A)$ , and  $j$  give transition energies, the value and one-standard deviation uncertainty of the Einstein  $A$  coefficients, and the total electronic angular momenta  $j$  of the excited states, respectively. A reference to the original data is given in columns labeled by "Ref.". Relevant thulium lines for which oscillator strengths are available can be found in Table VII.

$\Delta E/hc$ ( $\text{cm}^{-1}$ )	$A$ ( $10^6 \text{ s}^{-1}$ )	$u(A)$	$j$	Ref.	$\Delta E/hc$ ( $\text{cm}^{-1}$ )	$A$ ( $10^6 \text{ s}^{-1}$ )	$u(A)$	$j$	Ref.
16742.237	0.147	0.02646	7/2	[45]	29260.590	5.28	0.264	7/2	[61]
16957.006	0.651	0.03255	7/2	[61]	29316.690	9.80	0.49	9/2	[61]
17343.374	0.388	0.03104	7/2	[61]	30082.180	0.089	0.01157	5/2	[61]
17613.659	1.30	0.065	9/2	[61]	30124.020	0.615	0.05535	7/2	[61]
17752.634	1.09	0.0545	5/2	[61]	30302.420	1.61	0.1127	5/2	[61]
18837.385	2.17	0.1085	9/2	[61]	30915.020	4.29	0.2145	9/2	[61]
19548.834	0.241	0.03615	5/2	[61]	31431.880	3.82	0.191	5/2	[61]
19748.543	0.049	0.00882	9/2	[45]	31440.540	1.04	0.052	9/2	[61]
19753.830	0.398	0.03184	7/2	[61]	31510.240	15.9	1.272	7/2	[61]
21120.836	2.0	0.1	7/2	[61]	32174.490	1.50	0.135	5/2	[61]
21161.401	0.421	0.02105	5/2	[61]	32446.260	17.5	1.225	7/2	[61]
21737.685	0.518	0.0259	9/2	[61]	32811.020	16.1	1.127	7/2	[45]
22791.176	3.71	0.1855	7/2	[61]	33623.780	21.7	1.085	7/2	[61]
22929.717	12.0	0.6	5/2	[61]	34085.200	11.3	1.13	5/2	[61]
23781.698	24.3	1.215	9/2	[61]	34297.170	9.44	1.1328	7/2	[61]
23873.207	64.0	3.2	7/2	[61]	35026.220	24.2	1.936	5/2	[61]
24348.692	63.6	3.18	9/2	[61]	35261.762	1.13	0.2034	5/2	[45]
24418.018	97.9	4.895	5/2	[61]	37576.866	0.46	0.0828	9/2	[45]
25656.019	2.95	0.1475	5/2	[61]	37711.074	0.38	0.0684	9/2	[45]
25717.197	37.2	1.86	7/2	[61]	38120.710	5.2	0.936	9/2	[45]
25745.117	106	5.3	5/2	[61]	38128.370	0.62	0.1116	5/2	[45]
26126.907	2.94	0.147	5/2	[61]	38433.920	14.9	1.043	5/2	[45]
26439.491	0.806	0.05642	7/2	[61]	38502.000	14.0	0.98	9/2	[45]
26646.214	17.4	1.392	9/2	[61]	38696.790	3.5	0.63	5/2	[45]
26701.325	99.0	4.95	7/2	[61]	39161.450	36.8	2.576	7/2	[45]
26889.125	144	7.2	9/2	[61]	39206.840	2.7	0.486	9/2	[45]
28024.010	3.80	0.19	9/2	[61]	39547.310	6.4	1.152	5/2	[45]
28051.370	8.99	0.4495	5/2	[61]	39560.410	14.7	1.029	7/2	[45]
28448.585	1.42	0.071	5/2	[61]	39768.790	5.29	0.2645	9/2	[61]
28555.799	0.668	0.04008	7/2	[61]					

TABLE IX. Correlation coefficients  $r(C_k^{(i)}, C_l^{(j)})$  among four of the seven dispersion coefficients  $C_k^{(i)}$  of  $\text{Er}_2$  and  $\text{Tm}_2$ . Their values and uncertainties are given in Table I of the main text. Coefficients are labeled by rank  $k$  and index  $i$  following the notation in the main text. Correlation coefficients with the remaining three dispersion coefficients follow from the exact algebraic relationships among the dispersion coefficients.

Homonuclear Erbium dimer				
$k, i \setminus l, j$	Correlation coeff.			
	0,1	2,1	0,2	0,3
0,1	1.00	-0.38	-0.50	0.32
2,1	-0.38	1.00	0.37	-1.00
0,2	-0.50	0.37	1.00	-0.34
0,3	0.32	-1.00	-0.34	1.00

Homonuclear Thulium dimer				
$k, i \setminus l, j$	Correlation coeff.			
	0,1	2,1	0,2	0,3
0,1	1.00	-0.03	0.15	0.05
2,1	-0.03	1.00	-0.10	-1.00
0,2	0.15	-0.10	1.00	0.09
0,3	0.05	-1.00	0.09	1.00

- 
- [1] A. Griesmaier, J. Werner, S. Hensler, J. Stuhler, and T. Pfau, “Bose-Einstein condensation of chromium,” *Phys. Rev. Lett.* **94**, 160401 (2005).
- [2] T. Lahaye, C. Menotti, L. Santos, M. Lewenstein, and T. Pfau, “The physics of dipolar bosonic quantum gases,” *Rep. Prog. Phys.* **72**, 126401 (2009).
- [3] Mingwu Lu, Q. Burdick, Nathaniel, Seo Ho Youn, and Benjamin L. Lev, “Strongly dipolar Bose-Einstein condensate of dysprosium,” *Phys. Rev. Lett.* **107**, 190401 (2011).
- [4] K. Aikawa, A. Frisch, M. Mark, S. Baier, A. Rietzler, R. Grimm, and F. Ferlaino, “Bose-Einstein condensation of erbium,” *Phys. Rev. Lett.* **108**, 210401 (2012).
- [5] A. Frisch, K. Aikawa, M. Mark, A. Rietzler, J. Schindler, E. Zupanic, R. Grimm, and F. Ferlaino, “Narrow-line magneto-optical trap for erbium,” *Phys. Rev. A* **85**, 051401(R) (2012).
- [6] M. Lu, N. Q. Burdick, and B. L. Lev, “Quantum degenerate dipolar Fermi gas,” *Phys. Rev. Lett.* **108**, 215301 (2012).
- [7] A. de Paz, A. Sharma, A. Chotia, E. Maréchal, J. H. Huckans, P. Pedri, L. Santos, O. Gorceix, L. Vernac, and B. Laburthe-Tolra, “Nonequilibrium quantum magnetism in a dipolar lattice gas,” *Phys. Rev. Lett.* **111**, 185305 (2013).
- [8] S. Baier, M. J. Mark, D. Petter, K. Aikawa, L. Chomaz, Z. Cai, M. Baranov, P. Zoller, and F. Ferlaino, “Extended Bose-Hubbard models with ultracold magnetic atoms,” *Science* **352**, 201–205 (2016).
- [9] G. Natale, R. M. W. van Bijnen, A. Patscheider, D. Petter, M. J. Mark, L. Chomaz, and F. Ferlaino, “Excitation spectrum of a trapped dipolar supersolid and its experimental evidence,” *Phys. Rev. Lett.* **123**, 050402 (2019).
- [10] Alexander Petrov, E. Tiesinga, and Svetlana Kotochigova, “Anisotropy-induced Feshbach resonances in a quantum dipolar gas of highly magnetic atoms,” *Phys. Rev. Lett.* **109**, 103002 (2012).
- [11] S. Kotochigova, “Controlling interactions between highly magnetic atoms with Feshbach resonances,” *Rep. Prog. in Phys.* **77**, 093901 (2014).
- [12] A. Frisch, M. Mark, K. Aikawa, F. Ferlaino, J. L. Bohn, C. Makrides, A. Petrov, and S. Kotochigova, “Quantum chaos in ultracold collisions of gas-phase erbium atoms,” *Nature* **507**, 475–479 (2014).
- [13] T. Maier, H. Kadau, M. Schmitt, M. Wenzel, I. Ferrier-Barbut, T. Pfau, A. Frisch, S. Baier, K. Aikawa, L. Chomaz, M. J. Mark, F. Ferlaino, C. Makrides, E. Tiesinga, A. Petrov, and S. Kotochigova, “Emergence of chaotic scattering in ultracold Er and Dy,” *Phys. Rev. X* **5**, 041029 (2015).
- [14] C. Makrides, M. Li, E. Tiesinga, and S. Kotochigova, “Fractal universality in near-threshold magnetic lanthanide dimers,” *Science Advances* **4**, eaap8308 (2018).
- [15] A. Frisch, M. Mark, K. Aikawa, S. Baier, R. Grimm, A. Petrov, S. Kotochigova, G. Quémener, M. Lepers, O. Dulieu, and F. Ferlaino, “Ultracold dipolar molecules composed of strongly magnetic atoms,” *Phys. Rev. Lett.* **115**, 203201 (2015).
- [16] D. Sukachev, A. Sokolov, K. Chebakov, A. Akimov, S. Kanorsky, N. Kolachevsky, and V. Sorokin, “Magneto-optical trap for thulium atoms,” *Phys. Rev. A* **82**, 011405 (2010).
- [17] V. A. Khlebnikov, D. A. Pershin, V. V. Tsyganok, E. T. Davletov, I. S. Cojocar, E. S. Fedorova, A. A. Buchachenko, and A. V. Akimov, “Random to chaotic statistic transformation in low-field Fano-Feshbach res-

- onances of cold thulium atoms,” *Phys. Rev. Lett.* **123**, 213402 (2019).
- [18] L. N. Gorokhov, A. M. Emelyanov, and Y. S. Khodeev, “Mass-spectroscopic investigation of stability of gaseous molecules of  $\text{U}_2\text{O}_2$  and  $\text{U}_2$ ,” *High Temp.* **12**, 1156–1158 (1997).
- [19] M. Pepper and B. E. Bursten, “Ab initio studies of the electronic structure of the diuranium molecule,” *J. Am. Chem. Soc.* **112**, 7803–7804 (1990).
- [20] L. Gagliardi and B. O. Roos, “Quantum chemical calculations show that the uranium molecule  $\text{U}_2$  has a quintuple bond,” *Nature* **433**, 848–851 (2005).
- [21] Stefan Knecht, Hans Jørgen Aa. Jensen, and Trond Saue, “Relativistic quantum chemical calculations show that the uranium molecule  $\text{U}_2$  has a quadruple bond,” *Nat. Chem.* **11**, 40–44 (2019).
- [22] A. A. Buchachenko, G. Chałasiński, and M. M. Szcześniak, “Interactions of lanthanide atoms: Comparative ab initio study of  $\text{YbHe}$ ,  $\text{Yb}_2$  and  $\text{TmHe}$ ,  $\text{TmYb}$  potentials,” *Eur. Phys. J. D* **45**, 147–153 (2007).
- [23] M. Tomza, “Ab initio properties of the ground-state polar and paramagnetic europium–alkali-metal-atom and europium–alkaline-earth-metal-atom molecules,” *Phys. Rev. A* **90**, 022514 (2014).
- [24] A. Dunning, A. Petrov, S. J. Schowalter, P. Puri, S. Kotochigova, and E. R. Hudson, “Photodissociation spectroscopy of the dysprosium monochloride molecular ion,” *J. Chem. Phys.* **143**, 124309 (2015).
- [25] M. L. González-Martínez and P. S. Żuchowski, “Magnetically tunable Feshbach resonances in  $\text{Li}+\text{Er}$ ,” *Phys. Rev. A* **92**, 022708 (2015).
- [26] Klaudia Zaremba-Kopczyk, Piotr S. Żuchowski, and Michał Tomza, “Magnetically tunable Feshbach resonances in ultracold gases of europium atoms and mixtures of europium and alkali-metal atoms,” *Phys. Rev. A* **98**, 032704 (2018).
- [27] Maciej B Kosicki, Mateusz Borkowski, and Piotr S Żuchowski, “Quantum chaos in Feshbach resonances of the  $\text{ErYb}$  system,” *New J. Phys.* **22**, 023024 (2020).
- [28] Michał Śmiałkowski and Michał Tomza, “Highly polar molecules consisting of a copper or silver atom interacting with an alkali-metal or alkaline-earth-metal atom,” *Phys. Rev. A* **103**, 022802 (2021).
- [29] A. S. P. Gomes, T. Saue, L. Visscher, H. J. Aa. Jensen, R. Bast, *et al.*, (2019), DIRAC, A relativistic *ab-initio* electronic structure program, Release DIRAC19, Available at <http://dx.doi.org/10.5281/zenodo.3572669> and <http://www.diracprogram.org>.
- [30] Paweł Tecmer, Katharina Boguslawski, Mateusz Borkowski, Piotr S. Żuchowski, and Dariusz Kędziera, “Modeling the electronic structures of the ground and excited states of the ytterbium atom and the ytterbium dimer: A modern quantum chemistry perspective,” *Int. J. Quantum Chem.* **119**, e25983 (2019).
- [31] Robin Santra and Chris H. Greene, “Tensorial analysis of the long-range interaction between metastable alkaline-earth-metal atoms,” *Phys. Rev. A* **67**, 062713 (2003).
- [32] D. M. Brink and G. R. Satchler, *Angular momentum*, 3rd ed. (Clarendon Press, Oxford, 1993).
- [33] In the literature quadrupole moments are often defined to be twice  $\mathcal{Q}$ ; the quadrupole operator  $Q_{2q}$ , however, has a unique definition. See, for example, Sec. 4.10 of Ref. [32].
- [34] Svetlana Kotochigova and Alexander Petrov, “Anisotropy in the interaction of ultracold dysprosium,” *Phys. Chem. Chem. Phys.* **13**, 19165 (2011).
- [35] In this section we have implicitly made a change in coordinate system, where  $\mathbf{R}$  is now the separation between the center of masses of the atoms rather than the separation between the nuclei. Similarly, we use atomic rather than nuclear masses in the kinetic energy operator. These “non-adiabatic” changes are not considered significant in light of the uncertainties of our interaction potentials.
- [36] Daniel T. Colbert and William H. Miller, “A novel discrete variable representation for quantum mechanical reactive scattering via the S-matrix Kohn method,” *J. Chem. Phys.* **96**, 1982–1991 (1992).
- [37] Peter J. Knowles, Claudia Hampel, and Hans-Joachim Werner, “Coupled cluster theory for high spin, open shell reference wave functions,” *J. Chem. Phys.* **99**, 5219–5227 (1993).
- [38] M. Dolg, H. Stoll, and H. Preuss, “Energy-adjusted ab initio pseudopotentials for the rare earth elements,” *J. Chem. Phys.* **90**, 1730–1734 (1989).
- [39] X. Cao and M. Dolg, “Segmented contraction scheme for small-core lanthanide pseudopotential basis sets,” *Comput. Theor. Chem.* **581**, 139–147 (2002).
- [40] J. Visscher, O. Visser, P.J.C. Aerts, H. Merenga, and W.C. Nieuwpoort, “Relativistic quantum chemistry: the MOLFDIR program package,” *Comput. Phys. Commun.* **81**, 120 – 144 (1994).
- [41] G. Herzberg, *Molecular Spectra and Molecular Structure. Volume I: Spectra of Diatomic Molecules* (Van Nostrand Reinhold, New York, 1950).
- [42] J. T. Hougen, *The calculation of rotational energy levels and rotational line intensities in diatomic molecules* (1970) NBS monograph 115; See <https://doi.org/10.6028/NBS.MONO.115>.
- [43] W. J. Huang, G. Audi, M. Wang, F. G. Kondev, S. Naimi, and X. Xu, “The AME2016 atomic mass evaluation (I),” *Chin. Phys. C* **41**, 030002 (2017).
- [44] M. Wang, G. Audi, F.G. Kondev, W.J. Huang, S. Naimi, and X. Xu, “The AME2016 atomic mass evaluation (II),” *Chin. Phys. C* **41**, 030003 (2017).
- [45] A. Kramida, Yu. Ralchenko, J. Reader, and NIST ASD Team, (2019), NIST Atomic Spectra Database (version 5.7.1). Available: <https://physics.nist.gov/asd>. National Institute of Standards and Technology, Gaithersburg, MD.
- [46] J. F. Stanton, J. Gauss, L. Cheng, M. E. Harding, D. A. Matthews, P. G. Szalay, *et al.*, (2014), CFOUR, a quantum chemical program package. For the current version, see <http://www.cfour.de>.
- [47] H.-J. Werner, P. J. Knowles, G. Knizia, F. R. Manby, M. Schütz, *et al.*, (2015), MOLPRO, version 2015.1, a package of *ab-initio* programs. See <https://www.molpro.net>.
- [48] Hiroshi Akima, “A method of univariate interpolation that has the accuracy of a third-degree polynomial,” *ACM Trans. Math. Softw.* **17**, 341–366 (1991).
- [49] Jianmin Tao, John P. Perdew, and Adrienn Ruzsinszky, “Accurate van der Waals coefficients from density functional theory,” *Proc. Natl. Acad. Sci. U.S.A* **109**, 18–21 (2012).
- [50] D. Feller and K. A. Peterson, “Probing the limits of accuracy in electronic structure calculations: Is theory capable of results uniformly better than “chemical accu-

- racy”?” *J. Chem. Phys.* **126**, 114105 (2007).
- [51] M. Kodrycka and K. Patkowski, “Platinum, gold, and silver standards of intermolecular interaction energy calculations,” *J. Chem. Phys.* **151**, 070901 (2019).
- [52] A. Stone, *The Theory of Intermolecular Forces*, 2nd ed. (Oxford University Press, 2013).
- [53] Andrei Derevianko, Sergey G. Porsev, and James F. Babb, “Electric dipole polarizabilities at imaginary frequencies for hydrogen, the alkali-metal, alkaline-earth, and noble gas atoms,” *Atomic Data and Nuclear Data Tables* **96**, 323–331 (2010).
- [54] A. R. Edmonds, *Angular momentum in quantum mechanics*, 3rd ed. (Princeton University Press, 1957).
- [55] J. E. Lawler, J.-F. Wyart, and E. A. Den Hartog, “Atomic transition probabilities of Er I,” *J. Phys. B* **43**, 235001 (2010).
- [56] W. F. Meggers, C. H. Corliss, and B. F. Scribner, *Tables of Spectral-Line Intensities* (1975) NBS monograph 145; See <https://nvlpubs.nist.gov/nistpubs/Legacy/MONO/nbsmonograph145p1.pdf> and <https://nvlpubs.nist.gov/nistpubs/Legacy/MONO/nbsmonograph145p2.pdf>. Electronic data retrieved from <https://www.cfa.harvard.edu/amp/ampdata/kurucz23/sekur.html>.
- [57] V. N. Gorshkov and V. A. Komarovskii, “Lifetime of excited levels and oscillator strengths of Er I and Er II spectral lines,” *Opt. Spectrosc.* **50**, 853–857 (1981).
- [58] V. A. Komarovskii and Yu M. Smirnov, “Transition probabilities for the Er atom,” *Opt. Spectrosc.* **75**, 225–227 (1993).
- [59] J. E. Lawler, private communication (2012), The  $j = 5$  erbium excited state with energy  $hc \times 19201.343 \text{ cm}^{-1}$  above the ground state has a lifetime of 1700(170) ns and branching ratio of 0.9 to the ground state.
- [60] F. Ferlino, private communication (2012), The Einstein  $A$  coefficient of the  $j = 7$  erbium excited state with energy  $hc \times 24943.272 \text{ cm}^{-1}$  above the ground state has been supplied by the author.
- [61] M. E. Wickliffe and J. E. Lawler, “Atomic transition probabilities for Tm I and Tm II,” *J. Opt. Soc. Am. B* **14**, 737–753 (1997).
- [62] N. P. Penkin and V. A. Komarovskii, *J. Quant. Spectrosc. RA* **16**, 217–252 (1976), Electronic data retrieved from <https://www.cfa.harvard.edu/amp/ampdata/kurucz23/sekur.html>.